Doctoral Dissertation

The mechanism of emotion regulation in response to stress using an fMRI study and a biological mathematical model

Yukihiro Suzuki

September 12, 2022

Graduate School of Information Science
Nara Institute of Science and Technology

A Doctoral Dissertation
submitted to Graduate School of Information Science,
Nara Institute of Science and Technology
in partial fulfillment of the requirements for the degree of
Doctor of ENGINEERING

Yukihiro Suzuki

Thesis Committee:

Professor Kazushi Ikeda	(Supervisor)
Professor Matsumoto Kenichi	(Co-supervisor)
Professor Motoaki Kawanabe	(Co-supervisor)
Assistant Professor Makoto Fukushima	(Co-supervisor)
Project Associate Professor Saori Tanaka	(Co-supervisor)
Professor Yuichi Sakumura	(Co-supervisor)
Assistant Professor Jaymar Soriano	(University of the Philippines Diliman)

The mechanism of emotion regulation in response to stress using an fMRI study and a biological mathematical model*

Yukihiro Suzuki

Abstract

Stress is inevitable in our society. The ability to cope appropriately with the stress of social life is essential for adapting to complex environments. However, it is still unclear which brain regions and neural level characteristics contribute appropriately to adaptive responses under stress. The thesis examined two approaches to investigate the mechanisms of adaptation processing under stress by brain studies using fMRI and neuronal simulations.

First, during emotional regulation under stress in fMRI studies, the ventromedial prefrontal cortex (vmPFC) and pre-SMA showed significantly different activity in response to image valence. The midbrain showed differences with and without stress during assessing emotional images. Significant negative correlations with trait anxiety were confirmed for vmPFC, and correlations were obtained for pre-SMA, mainly for negative affect. Furthermore, functional coupling between vmPFC and midbrain was negatively correlated with acute stress-induced changes in anxiety. These results indicate that activity and functional connectivity, including vmPFC, in emotion regulation reflect individual differences in response to stress.

Second, we focused on two distinctive firing types to understand the locus coeruleus (LC) mechanisms, a noradrenergic resource that is important for controlling the arousal that occurs in stress. We assumed two modes, homogeneous and inhomogeneous, to understand how these firing characteristics function as a

*Doctoral Dissertation, Graduate School of Information Science,
Nara Institute of Science and Technology, September 12, 2022.

neural population. Combining these modes with a feed-forward neural network model revealed that the homogeneous mode detects more significant spike coherence than the inhomogeneous mode. On the other hand, the inhomogeneous mode was found to have the ability to suppress spike coherence. These functions support previous studies in biological experiments, indicating that these two modes are dynamically responsible for controlling cognitive processing, including stress.

Keywords:

fMRI, Stress, Emotion Regulation, Neural Population Coding, vmPFC, Locus coeruleus

fMRI研究と生物学的数理モデルを用いたストレスに応答する情動制御の仕組み*

鈴木文丈

内容梗概

私たちの社会ではストレスは避けられないものであるため、社会生活におけるストレスに適切に対処する能力は、複雑な環境に適応するために不可欠な能力である。しかし、どのような脳領域や神経レベルの特性がストレス下での適応反応に適切に寄与しているのかは、未だ不明である。本論文では、ストレス下での適応処理のメカニズムを解明するために、fMRIと神経細胞シミュレーションを用いた脳研究により、2つのアプローチを検討した。

まず、fMRI研究では、ストレス下における画像のvalenceに依存して、腹内側前頭前野（vmPFC）とpre-SMAが有意な活動を示した。また、中脳は情動画像の評価において、ストレスの有無による活動の差異を示した。その中でもvmPFCでは特性不安との有意な負の相関が確認され、pre-SMAでは主に負の情動に対して相関関係があった。さらに、vmPFCと中脳の機能的結合は、急性ストレスによる不安の変化と負の相関があった。これらの結果は、情動制御におけるvmPFCを含む活動や機能的結合がストレスに対する反応の個人差を反映していることを示している。

次に、ストレス時に生じる覚醒を制御するために重要なノルアドレナリン資源である青斑核（LC）機構を理解するために、2つの特徴的な発火特性に注目した。これらの発火特性が神経集団としてどのように機能するかを理解するために、均質と非均質の2つのモードを仮定した。これらのモードをフィードフォワードニューラルネットワークモデルと組み合わせることで、均質モードは非均質モードよりも大きなスパイクコヒーレンスを検出することが判明した。一方で、非均質モードはスパイクのコヒーレンスを抑制する機能を持つことが示された。これらの機能は、生体実験で示された複数の先行研究を支持するものであり、この2

*奈良先端科学技術大学院大学 情報科学研究科 博士論文,
September 12, 2022.

つのモードがストレスを含む認知処理の制御に動的に関与していることを示している。

キーワード

fMRI, ストレス, 情動制御, 集団神経細胞モデル, 腹内側前頭前野, 青斑核

Acknowledgements

First of all, I would like to thank my primary supervisor, Prof. Kazushi Ikeda of the Laboratory of Mathematical Informatics, for his prompt response to various application forms and other requests despite his busy schedule. Thanks to his help, I could smoothly devote myself to my research without any particular difficulties.

I am grateful to Dr. Saori Tanaka, head of the Mathematical Intelligence Laboratory (NCD) at the Brain Information Laboratory of the Advanced Telecommunications Research Institute International (ATR). She often advised me on various research advice regarding the advising professor and co-author in the Computational Neuroscience Laboratory. In particular, I would like to express my sincere gratitude for her excellent help in checking the journal, ethics application, and presentation materials for our fMRI research.

I would like to thank Prof. Yuichi Sakumura for his advice on the neural population coding study. While I was busy with work, he was flexible in making time for me and gave me numerous suggestions. Thank you also for your friendly support when I struggled to reproduce the simulation.

I also thank the thesis committee, including Prof. Kenichi Matsumoto, Prof. Motoaki Kawanabe, Dr. Makoto Fukushima, and Dr. Jaymar Soriano, for giving me valuable comments.

In the Laboratory of Mathematical Informatics, Prof. Junichiro Yoshimoto, Dr. Atkatomi Kubo, and Dr. Takashi Nakano (Fujita Health University) advised my research and consulted with my various research life. Aya Tanimoto and Sachiko Yasuki help me for my student life as the secretaries.

I would like to thank members of ATR, Dr. Yuki Sakai and Dr. Issaku Kawashima (ATR-NCD), for many valuable comments on my research. Dr. Kana Inoue and Dr. Kaori Tach support my research for data collection and as the psy-

chologist in the stress test. I could not take the experiment without their help. I am grateful to Yuko Minami for supporting my research life as a secretary. I am also thankful to thank the support staff of ATR, especially Ikuhiro Shimada, Nambe Mieko, Kaori Nakamura, and other radiologists at BAIC. I could not carry out my research without their great help.

This fMRI study is the result of the project 'Science of personalized value development through adolescence: integration of brain, real-world and life-course approaches' (JP16H06396) of Grants-in-Aid for Scientific Research on Innovative Areas from the Japan Society for the Promotion of Science.

Finally, I would like to express my gratitude to my family for their moral support and warm encouragement.

Contents

List of Figures **ix**

List of Tables **x**

1 Introduction **1**

2 The fMRI Research of Emotion Regulation in Response to Stress **4**

2.1 Background 4

2.2 Materials and Methods 7

2.2.1 Experimental procedure. 7

2.2.2 Participants. 8

2.2.3 Stress-induced test. 9

2.2.4 Emotion evalution in the fMRI task. 9

2.2.5 Measurement and analysis of salivary alpha-amylase. . . . 11

2.2.6 Measurement and analysis of the STAI. 12

2.2.7 MRI data acquisition. 12

2.2.8 MRI data pre-processing and statistical analysis. 13

2.2.9 Functional connectivity analysis. 14

2.2.10 Debriefing 14

2.2.11 Software and code 15

2.3 Results 16

2.3.1 Physiological and psychological response's result 16

2.3.2 Subjective evaluation in the fMRI task 17

2.3.3 fMRI imaging result 17

2.3.4 Functional connectivity for ROI-to-ROI analysis 21

2.4 Discussion 23

3 Two modes in locus coeruleus have essential roles for stimulus encoding 27
3.1 Background 27
3.2 Materials and Methods 31
3.2.1 Network Architecture 31
3.2.2 LC model 32
3.2.3 Neuron model 33
3.2.4 Synapse model 34
3.2.5 Measurement of the histogram and spike coherence 35
3.3 Results 36
3.3.1 Histogram results 36
3.3.2 Spike Coherence results 37
3.3.3 Noise enhancement 38
3.3.4 The rate change in homogeneous and inhomogeneous modes 39
3.4 Discussion 40

4 General Discussion 43

5 Supplementary Information 46

References 48

List of Figures

2.1 Experimental design and fMRI task. 7
2.2 Trier social stress test(TSST) in progress 9
2.3 Salivary alpha-amylase levels and anxiety test. 16
2.4 Subjective evaluation in the fMRI task. 18
2.5 Whole-brain analysis. 19
2.6 Correlation analysis in the vmPFC and pre-SMA. 20
2.7 ROI-to-ROI analysis. 22

3.1 Examples of membrane potential to tonic and phasic signal. . . . 28
3.2 Five-layer's feed-forward network model (network architecture). . 31
3.3 The signal frequency changes in a sinusoidal manner. 32
3.4 Overview of our hypothesis model. 33
3.5 Raster plots and histograms of the homogeneous mode. 36
3.6 Histograms of the homogeneous and inhomogeneous modes. . . . 37
3.7 Spike coherence of the model network. 38
3.8 Enhancement for the LC models input frequency. 38
3.9 The rating between homogeneous and inhomogeneous modes. . . . 39

5.1 Spike coherence and value of OU process when varying σ 46

List of Tables

2.1 The number of images of valence and category used in NAPS BE 11
2.2 SPM results for main effects of valence and stress 21

1 Introduction

The environment around us is very complex and constantly changing. These changes can be large or small, long or short. For example, some changes, such as entering an educational institution or transferring to a rural area, are significant in one's environment. Others, such as preparing for final exams, make one's life around them study-centered for a certain period. In addition, these changes can be broadly separated into those that affect us psychologically and those that affect us physically. Thus, life is constantly undergoing various changes. We adapt to our complex environment by taking appropriate responses to these changes.

Although we experience many external environmental stimuli, many external stimuli can be presented as stress responses. Stress is defined as a deviation from a steady or resting state. The stimulus that causes stress response is recognized as a stressor [1,2]. It would be significant how we internally perceive and interpret stress and adapt to our environment from a cognitive and medical perspective.

It has been noted that there are various ways of adapting to stress. For example, some may adapt to maintain their current situation by keeping homeostasis [3]. Also, since stressful events are easily remembered, brain activity may be activated in response to the event to prepare for similar stressful events in the future [4]. Such behaviors that minimize the effects of stress are defined as coping, and appropriate coping can contribute to fear detection, homeostasis, and survival performance. However, some people may lack these abilities because stress coping is variable and individual-dependent depending on the situation. It suggests that dysfunctional stress adaptation can make it difficult for attention, memory storage, and complex decisions. In some cases, stress may put individuals at risk for developing a variety of mental disorders, such as anxiety disorder and depression, Etc [5,6].

Therefore, various previous studies have provided several ways of dealing with

how we process and adapt to stress. However, the detailed mechanisms at the brain and neuronal population level in response to stress are unknown. To address these issues, we divided our investigation into macroscopic approaches to brain regions and microscopic approaches at the neuronal level as follows,

- From fMRI studies in emotional regulation under stress, we investigated how brain regions are related to and interact with stress and emotional regulation and respond to stress. We performed an fMRI experiment of an emotional evaluation task to investigate the background. Participants were stressed by the stress interview; following the fMRI task, they viewed emotional images and rated their emotional strength, including six basic emotions and preferences. The results revealed that the ventromedial prefrontal cortex (vmPFC) was correlated with behavioral measures reflecting individual differences in response to stress. Furthermore, there is significant functional connectivity between the vmPFC and the midbrain only under stress, and the strength of this coupling reflected individual differences in stress-induced emotional regulation.

- We found that the midbrain close to locus coeruleus(LC) showed the main effect of stress. And then, the functional connectivity between vmPFC and midbrain showed the individual difference in stress effect from the fMRI study. However, it is unclear how the mechanism within brain regions is caused by individual differences in stress response, especially neural level. In this study, we focused on locus coeruleus, which were close to the midbrain we detected in the fMRI study. LC is a significant resource of noradrenaline and is closely related to stress. LC adapts to stress by appropriately using phasic and tonic signals depending on the stress presence/absence situation. In our study, we assumed that the overlapping of each signal defines the homogeneous and inhomogeneous modes. We analyzed whether the stimuli are encoded by a feed-forward network model for using the modulator. As a result, we found that the differential information of the stimulus is appropriately encoded in the homogeneous mode. In contrast, the differential information is challenging to encode in the inhomogeneous mode. It suggests that the homogeneous mode in LC can be applied to quick response.

However, the inhomogeneous mode suppresses the spike coherence. It can be helpful to mental disorders by suppressing excessive spike coherence occurred by an excessive stressor. And then, these modes can be a factor in the individual difference in our cognition occurred by stress.

Finally, in the general discussion, we propose a hypothesized mechanism based on the results of the fMRI and simulation studies above. From the fMRI study, when the change in state anxiety in response to acute stress is significant, the functional coupling between the vmPFC and the midbrain, including LC, is negative. In this case, vmPFC activity can be decreased, and midbrain activity, including the LC, can be increased. And then, from the simulation study, when stress coping is not successful, the homogeneous mode may become dominant in the LC, which increases the overall activity of the LC. This mechanism supports previous studies and provides a possible mechanism linking the vmPFC and the LC in response to stress.

In Chapter 2, we describe fMRI research on emotion regulation under stress. And then, in Chapter 3, to model the mechanism of stress in LC from the population level, we conducted the simulation study using the biological mathematical model in a feedforward network with intra-layer random connections. Finally, Chapter 4 provides conclusions and future perspectives.

2 The fMRI Research of Emotion Regulation in Response to Stress

2.1 Background

In our social lives, we are constantly exposed to the stress response. When stress occurs, we often experience negative emotions such as fear, sadness, and anxiety. When stress causes negative emotions, many people cope appropriately by regulating their emotions. There are various ways to suppress these negative emotions caused by external factors, but how stress affects such cognitive control is unexplored.

Emotions shape how we think, feel, and behave. Emotions are also organized as cognitive, subjective, and physiological sets of positive or negative values thought by an individual in a particular context and are regulated in various ways. In contrast to these emotions, emotion regulation is defined as an attempt to monitor and regulate the emotional experience, triggered when the emotional response is subject to evaluation or when conflicts arise between different emotional responses [7–9]. Emotion regulation is associated with various cognitive functions and is thought to influence risk behavior reduction, cognitive reappraisal, and social decision-making paradigms [10–12]. Impairments in emotion regulation are seen in patients with psychiatric disorders such as depression and autism spectrum disorders and adjustment disorders characterized by an exaggerated response to stress [13, 14].

Emotional control is associated with the default mode network (DMN) at the neural network level. Dysfunction of DMN may lead to neuropsychiatric dis-

orders and may harm emotional control [15, 16]. The default mode network is involved in a variety of spontaneous and naturally processing and can be divided into two significant subsystems [17]. The first is the anterior part, associated with consciousness and memory processing, with the posterior cingulate cortex (PCC), which plays a central role. The second is the posterior part, which is associated with the self-referential process and emotion regulation, and the medial prefrontal cortex (mPFC) is a representative brain region. And then, each subregion of the mPFC has been shown to contribute different functions to the subsystems of the default mode network. For example, anterior mPFC (aMPFC) contributes to making self-other distinctions by coupling with the cingulate cortex [18, 19]. In particular, the ventral mPFC (vmPFC) is said to be involved in emotional engagement and has a crucial role in regulating emotion by controlling anxiety, fear extinction, and encoding emotional stimuli [20–24]. It has also been suggested that tagging information such as emotions related to themselves [25]. Detailed mechanisms of vmPFC in emotion regulation have also been investigated in both rodents and humans [26]. In humans, recent studies have suggested that vmPFC has a neurochemical function in emotion processing [27–30]. Furthermore, vmPFC is also associated with stress, suggesting dynamic changes in vmPFC during stress [31–33]. Activation of vmPFC was initially decreased by exposure to stressful images and then increased by stress coping. These findings suggest that vmPFC may be involved in adaptive responses, including emotion regulation during stress, but the detailed mechanisms are largely unknown.

We hypothesized that stress affects vmPFC activity, which affects the emotion regulation associated with the vmPFC. In addition, we hypothesized that this effect's level might influence individual differences in response to stress. To examine this hypothesis, we conducted an fMRI experiment in which participants were exposed to acute social stress, followed by an fMRI emotional task in which they viewed an emotional image and rated the emotional strength of that image. Based on the hypothesis, the vmPFC can be associated with emotional regulation given an emotional stimulus. And then, according to subsequent emotional evaluation, according to previous studies, the limbic system can be activated by emotional responses associated with emotional regulation [9, 22, 34]. However, some previous studies suggested that brain regions related to emotional stimuli

and responses can be mixed [35, 36]. Therefore, to investigate the complex function of the vmPFC, we focused on the activity and functional connectivity of the vmPFC while participants were viewing images and rating the strength of their emotional responses. To measure participants' level of psychological response to stress during the experiment, we asked them to complete the State-Trait Anxiety Inventory, a frequently used measure of stress. We found that the vmPFC was more activated at higher valence and that brain region associated with stress were also correlated with the emotional regulation of the vmPFC.

2.2 Materials and Methods

2.2.1 Experimental procedure.

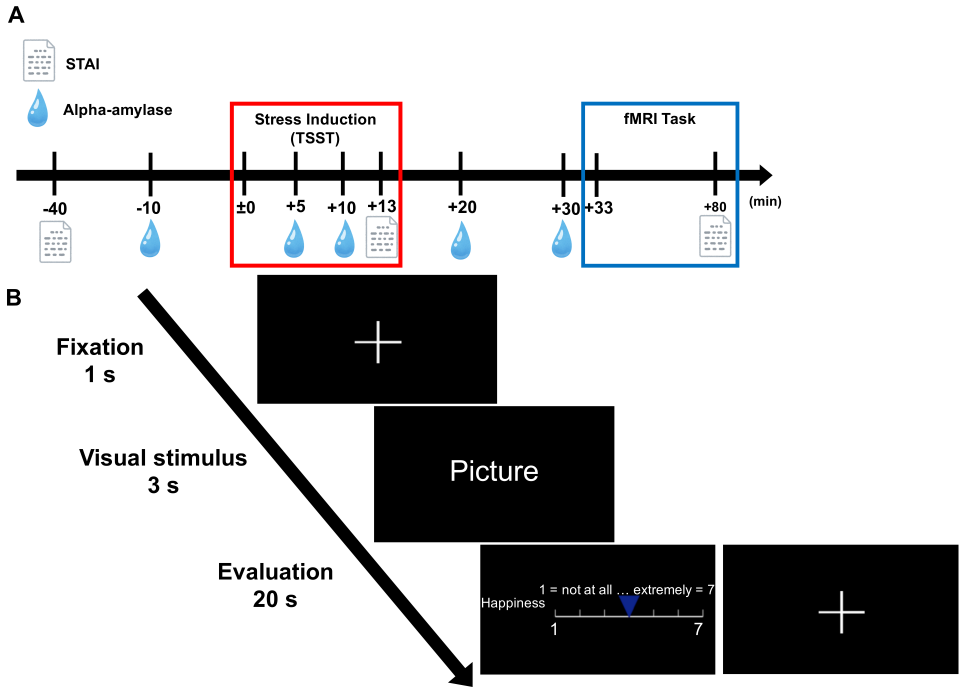

Figure 2.1: Experimental design and fMRI task. (A) Experimental Procedure. Onset (± 0 min) was defined as the start of the stress test. The schedule was the same for both stress and control conditions, but the content of the TSST was different in both conditions. (B) The fMRI task. Participants rated a psychological index consisting of basic emotions (happiness, sadness, fear, anger, disgust, surprise) and preferences on a 7-point scale in response to a displayed photographic image on the screen. Sessions were performed four times, and participants rated 19 images in each session.

All participants participated in the stress condition on the first experimental day and the control condition on the second experimental day. The interval between the first and second experimental days was five months. On the first experimental day, the experimenter explained the ethical and safety aspects of

the study to all participants. After obtaining informed consent, all participants were asked to rest for 20 minutes. They then experienced a 13-minute stress-induced test. After the stress-induced test, participants entered the fMRI scanner. They were asked to perform an emotional evaluation task (see Fig. 2.1A for the exact timing of measurements). STAI-JYZ and salivary α-amylase were measured repeatedly during the experiment. Following previous studies [37], to minimize diurnal variations in α-amylase secretion, salivary α-amylase was measured between 14:10 and 16:40. Thus, we performed all experiments between 13:30 and 17:30. The experimental sample was collected between September 2018 and June 2019.

2.2.2 Participants.

Because female stress responses are altered by menstrual cycles [38,39], measuring the saliva without the influences is difficult. Therefore, twenty-one participants were fixed to be male with right-handed (mean age $\pm$ SD, 23.10 $\pm$ 1.81 years; range, 21-28 years). And then, twenty-one participants without mental disorders, claustrophobia, or neuroendocrine disorders were recruited. Participants are between 18 and 30 years old, and recruitment was done by advertisements at Advanced Telecommunications Research Institute International. They were prohibited from consuming caffeine or citrus juices up to 4 hours before the experiment and alcohol 24 hours before the experiment. In addition, they were checked for the use of corticosteroids and antipsychotic drugs and prohibited excessive exercise, food, and smoking at least 2 hours before the experiment. They also refrain from taking any medication for two weeks. Due to an omission in the State-Trait Anxiety Inventory-JYZ (STAI-JYZ), one participant was excluded from correlation and statistical analyses involving STAI-JYZ. Participants provided informed consent before the experiment, and ATR Review Board Ethics Committee approved all experimental procedures. All procedures were performed under relevant guidelines and regulations. Participants received 11,000 yen for a one-time experiment and joined two times in the experiments: stress and control condition.

2.2.3 Stress-induced test.

According to a previously published protocol, all participants underwent Trier Social Stress Test (TSST) [40, 41]. The TSST is a stress-induced test to give acute social stress. Fig shows a specific TSST, which is unique in that the stress is generated mainly by the constant monitoring of the subject by a video camera and interviewer.

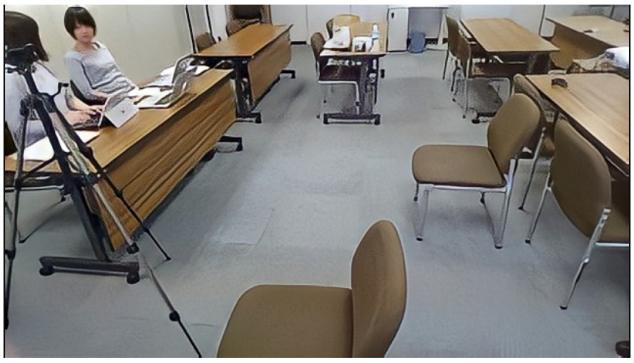

Figure 2.2: Trier social stress test(TSST) in progress

On the first day, participants performed TSST of stress condition. They prepared an interview about the future job (5 min), talked an interview speech (5 min), and performed a problematic math task (3 min). In this condition, they were interviewed by a clinical psychologist (certified in Japan) and were monitored from a video camera during the stress condition. And then, participants performed TSST in the control condition on the second day. They completed a placebo version of the TSST consisting of free speech (5 min), conversation (5 min), and a simple math task (3 min). Stress-induced test on the control condition, there is no clinical psychologist and a video camera. After all experiment procedures, we explained that a video camera was not recorded and used video camera to add stress.

2.2.4 Emotion evalution in the fMRI task.

The fMRI task will be administered 33 minutes after the start of the TSST. Participants will view natural photographic images in the MRI scanner and assess

their emotions and preferences in the images. Participants are asked to gaze at a fixation point for one second and then look at a visual stimulus (an image) for three seconds during one trial. Using a cursor, participants are then asked to rate their emotional response to the target image. The participants are asked to rate each item on a 7-point Likert scale within 20 seconds. If the respondent responds to all the indicators, a crossed-out viewpoint is displayed for the remainder of the time. Each trial lasts 24 seconds, and the participants are asked to evaluate 19 presented images during one session. Each experiment consists of 4 sessions and takes about 30 minutes. The pointer on the number line is manipulated using the reaction buttons on the brain activity imaging center(BAIC) in ATR for evaluation.

The images used are from the Nencki Affective Picture System (NAPS) [42]. NAPS is freely available for non-commercial use (http://naps.nencki.gov.pl/). It comprises 1356 images labeled for emotion rating (emotional valence/arousal), luminance, contrast, JPEG size, and entropy. They are further divided into five content categories: animals, landscapes, faces, people, and objects. Entropy is calculated from the histogram of each pixel intensity value x and written below. From this formula, entropy is expressed by the "randomness" of image contrast. It indicates that low-entropy images, such as dark scenes or the sea, were shown with uniform contrast.

$$H = -\Sigma p(x) \log p(x)$$

where p is the frequency of intensity x. It is expressed as the higher the entropy, the more random (more informative) the image.

In addition, 510 images contain emotion ratings (basic-emotion normative ratings: happiness, sadness, fear, surprise, anger, disgust + arousal, and emotional valence). These image sets are the basic-emotion normative ratings for the Nencki Affective Picture System (NAPS BE) [43]. We used 152 images from this set of 510 images in the experiment, 76 images for the stress condition and 76 images for the control condition. However, because NAPS contains some unpleasant images (images with high ratings of fear and disgust), the description of the NAPS image set will be included in the experimental instructions, and participants were informed of this fact before the experiment was conducted. All the data used in this experiment were based on previous studies of NAPS BE, and only images

that a single emotion component can cluster were used in this experiment. The valence of the NAPS dataset is scored from 1 to 9 points, and the images are classified based on the value of the valance, following previous studies, where 1-3 points are defined as N: Negative, 4-6 points as M: Medium, and 7-9 points as P: Positive. P: Positive. To prevent the Serial Position Effect (the effect of learning an image when it is presented multiple times of the same type or valence), the same valence category was presented up to twice and the same type category up to three times in a row. Table 2.1 shows the number of images used in the experiment by type and valence category.

The fMRI and evaluation analyses used the factors in a full-factorial design two-way repeated-measures ANOVA. The analytical design comprised within-participant factors of two conditions: one is stress and control conditions, and two is three image valences (negative, medium, and positive). An overview of each trial is shown in Fig. 2.1B (see ‘fMRI procedure’ in “Methods” for fMRI analysis information).

2.2.5 Measurement and analysis of salivary alpha-amylase.

To confirm the acute stress by TSST, alpha-amylase in saliva, one of the typical biomarkers for stress detection, was collected. Saliva samples were collected at five time points (-10 minutes, +5 minutes, +10 minutes, +20 minutes, and

Table 2.1: The number of images of valence and category used in NAPS BE

	Stress Condition			Control Condition		
Category/Valence	Negative	Medium	Positive	Negative	Medium	Positive
Animals	4	5	6	3	5	7
Faces	5	5	5	5	5	5
Landscapes	0	3	13	0	3	13
Objects	5	5	5	5	5	5
People	5	4	6	6	4	5
Total	19	22	35	19	22	35

+30 minutes) based on the onset (± 0 minutes) of TSST. Saliva can easily be collected with this device, and it only requires 1 min to determine alpha-amylase levels. Saliva was collected by placing a special sheet under the tongue for 30 seconds. The sheet was then placed in an amylase monitor (NIPRO, Japan) to measure amylase. The value measured from the device is kIU/L and is followed by an international unit (IU). We applied paired t-test between stress and control conditions.

2.2.6 Measurement and analysis of the STAI.

To assess psychological responses to acute social stress, participants were scored on the STAI for anxiety [44]. The STAI consists of a 20-item state anxiety scale and a 20-item trait anxiety scale, with participants rating each item on a scale of 1 to 4. In the experiment, we used the STAI-JYZ, an official Japanese-translated version of the STAI (form-Y) [45]. The STAI-Y1 is a 20-item state anxiety scale that assesses transient situational reactions to anxiety-provoking events. The STAI-Y2, on the other hand, is a 20-item trait anxiety scale used to evaluate relatively stable response tendencies to anxiety experiences. The STAI-JYZ was also measured three times: before the TSST (-40min), immediately after the TSST (+13min), and after the completion of the fMRI task (+80min), with the start of the TSST at ± 0 min. In statistical analysis, we applied two-way repeated-measures ANOVA to test for the effects of time on the measure and stress.

2.2.7 MRI data acquisition.

A 3-T MAGNETOM Prisma MRI system (Siemens) was used to acquire both structural T1-weighted images (repetition time = 2250 ms, echo time = 3.06 ms, flip angle = 9°, thickness = 1 mm, field of view=256 mm, slice gap=0 mm) and T2*-weighted echo-planar images (repetition time=2000 ms, echo time = 30 ms, flip angle = 80°, slices = 56, thickness = 2.5 mm, field of view = 200 mm, slice gap = 0 mm, multi-slice mode, interleaved). The area of acquisition is the whole brain scan. In T2*-weighted echo-planar images measured during the fMRI task, the 233 volumes are the total volume per session. Since there are four sessions

in this experiment, there are 233 × 4volumes, and the first five volumes in each session are excluded from the analysis as dummy scans. Participants did not take the fMRI task during the dummy scan and started watching valenced images after the dummy scan.

2.2.8 MRI data pre-processing and statistical analysis.

All fMRI image data were converted from DICOM format to NIfTI format for analysis. The first five scans were excluded as dummy scans for T2* image data scanned during the fMRI task. At first of preprocessing, The intermediate functional images in the session were initially used as reference images, and other functional images were realigned to the reference to compensate for head movement. The structural images were coregistered to correct the position of the functional images roughly. And then, the volumes were processed for segmentation and normalization. Finally, the functional images were smoothed using a Gaussian filter with an 8-mm full-width at a half-maximum Gaussian kernel.
The general linear model was applied to the pre-processed data. We focused on the BOLD signal in two intervals. The first is during the 3-s displayed image, and the second is during the 20-s evaluation of the image. Differently designed matrices were applied to the first-level GLM analysis for these two intervals. In each period, all trials were sorted based on image valence type (negative, medium, and positive) and were defined by three box-car regressors with a duration of 3 s (image display periods) or 20 s (evaluation periods). These factors were convolved with a hemodynamic response function (HRF). Therefore, we defined four first-level designed matrices for each participant: two periods (image display, evaluation) × two conditions (stress, control). The realignment parameters (three translations and three rotations) were added as multiple regressors of head movement. For the group-level (second-level) analysis, the fMRI data were subjected to a flexible factorial model with 2x2 levels of condition and valance. This model was applied separately in the image presentation and evaluation intervals. All group-level analysis results were corrected using cluster-level inference (cluster-defining threshold of $P < 0{:}001$, cluster probability of $P < 0{:}05$, FWE- corrected). Data were pre-processed and applied statistical analysis using Statistical Parametric Mapping 12 (SPM12, update revision number 7487, Wellcome Department

of Cognitive Neurology, London, UK, https://www.fil.ion.ucl.ac.uk/spm) toolbox and MATLAB 2018a (version 9.4.0, The MathWorks, Inc., Natick, Massachusetts, https://matlab.mathworks.com).

2.2.9 Functional connectivity analysis.

Functional connectivity analysis was performed using CONN (ver.17.f, https://web.conn-toolbox.org). Three brain regions were extracted from fMRI imaging data's whole-brain analysis as functional ROIs: the vmPFC, pre-SMA, and midbrain. The pre-SMA and vmPFC detected as clusters from the flexible factorial model were defined as ROI. However, the midbrain was extracted from a 5-mm radius area around the peak coordinates of the midbrain (MNI: x, y, z = -4, -32, -24). At first, fMRI imaging data was pre-processed following the order: realignment and unwarp, slice timing correction, segmentation, normalization, outlier detection, and smoothing (kernel FWHM of 8 mm). Outlier detection was applied to identify scans with motion more significant than the 95th percentile, and these outliers were denoised. Two methods were performed in denoising: 1) linear regression of the potential confounding factors of the BOLD signal, including the realignment parameters and scrubbing extracted from the outlier detection, and 2) temporal band-pass filtering. A first-level analysis was performed with each trial's valence and stress conditions as regressors (the analysis matrix setup was identical to the first-level analysis in SPM12). Regressors were convolved with HRFs. The ROI-to-ROI analysis was performed to calculate the Z-transformed correlation coefficient of the BOLD signal averaged over all voxels in the ROI. The analysis time was the evaluation period (20 seconds for each trial). We tested whether the functional connectivity between target ROIs was significantly greater than 0 in each stress and control condition.

2.2.10 Debriefing

In this experiment, we describe cognitive load instead of stress to prevent the subjects from recognizing that we will give them stress in the instructions for obtaining the subjects' consent. The details are given to the subjects after the experiment is completed. In addition, since the video camera is used for moni-

toring and not for analysis, the debriefing also explains this.

2.2.11 Software and code

In data collection, all image stimuli were presented with psychopy (Release 1.90.3) for presentation software, and all fMRI data were collected with a 3-T MAGNETOM Prisma MRI system (Siemens). Data analysis was processed using python3 with statsmodels(ver.0.9.0), MATLAB 2018a with Statistical Parametric Mapping 12 toolbox, and CONN toolbox (ver.17.f). Figure 2, Figure3, Figure 5, and Figure 6 were created with matplotlib(version 2.2.3), seaborn(version 0.9.0), and CONN toolbox (ver.17.f). Figure 4 was created using the Statistical Parametric Mapping 12 toolbox.

2.3 Results

2.3.1 Physiological and psychological response's result

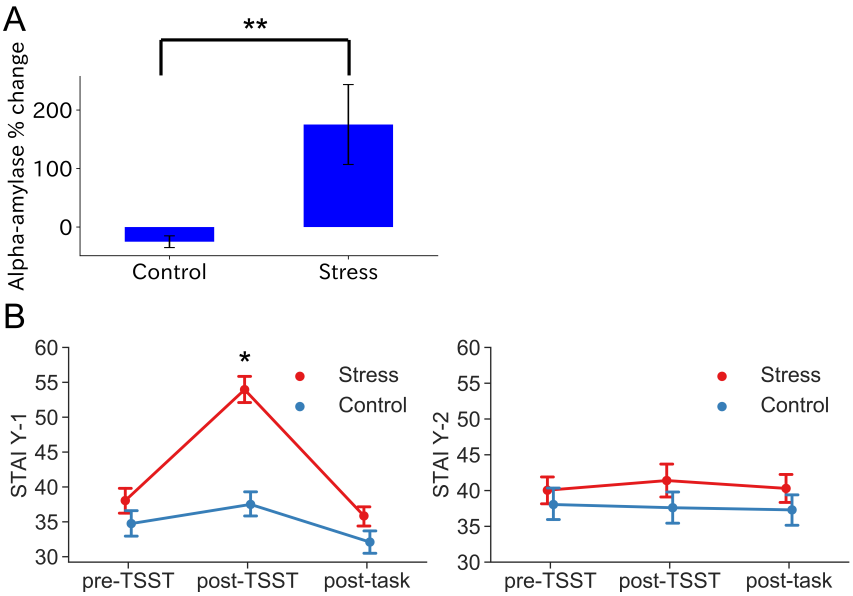

Figure 2.3: Salivary alpha-amylase levels and anxiety test. (A) Salivary alpha-amylase levels. Acute social stress significantly increased the alpha-amylase level ($P < 0.01$ on paired t-test). The alpha-amylase level represents the percent change between $-$ 10 min (before the TSST) and + 10 min (after the TSST speech). (B) STAI-Y1 (state anxiety) and STAI-Y2 (trait anxiety) scores. The STAI Y-1 showed a significant interaction between conditions (stress, control) and measurement time ($-$ 40 min, after the TSST, +80 min). ($F(2,114) = 8.68$, $P < 0.001$ in two-way repeated measures ANOVA). However, the STAI Y-2 showed no significant difference ($P > 0.05$). Error bars indicate s.e.m.

At first, we measured salivary alpha-amylase several times to check whether participants felt stressed by the experimental procedure to generate stress. Setting the onset as the start of the TSST, we collected saliva five times: -10min, +5min, +10min, +20min, and +30min. Under stress and control conditions, we

defined the baseline saliva value at -10min and calculated the percentage change in salivary alpha-amylase compared to $+10min$ (after the speech during TSST). Fig.2.3A showed that salivary alpha-amylase in stress condition significantly increased compared with the control condition ($t(20) = 3.09$, $P < 0.01$ on paired t-test). Thus, stress was thus successfully induced under the test conditions.

Next, to investigate the psychological effects of stress, we examined STAI-JYZ measured at -40min (before the TSST), +13min (after the TSST), and +80min (after the fMRI task) (Fig. 2.1A and "Materials and Methods"). We found the significant interaction between condition (stress, control) and measurement time (-40 min, +13 min, +80 min) for STAI-Y1 (state anxiety) ($F(2,114) = 8.68$, $P < 0.001$ on two-way repeated-measures ANOVA; Fig. 2.3B). On the other hand, no significant interaction or main effect was obtained for STAI-Y2 (trait anxiety). Furthermore, Tukey's HSD multiple comparison test showed that state anxiety differed between the stress and control conditions immediately after the stress-induced test (TSST) in the stress and control conditions. These results indicate that state anxiety induced by acute social stress is transient. Thus, a transient stress state was caused by the stress test.

2.3.2 Subjective evaluation in the fMRI task

A two-way repeated-measures ANOVA was performed on seven indicators of the six basic emotions and preferences. Valence factors were assigned to the images (negative, medium, positive) and conditions (stress, control). Sadness, anger, disgust, preference, and happiness showed significant interactions ($F(2,40) = 9.06$, $P < 0.001$; $F(2,40) = 2.82$, $P < 0.05$; $F(2,40) = 4.99$, $P < 0.01$; $F(2,40) = 3.81$, $P < 0.05$; $F(2,40) = 6.24$, $P < 0.01$, respectively, in two-way repeated measures ANOVA; Fig. 2.4). No interaction was found for fear and surprise, but fear showed the main effect on the condition ($F(2,20) = 7.89$, $P = 0.011$).

2.3.3 fMRI imaging result

In the fMRI whole-brain analysis, an ANOVA model with valence (negative, medium, positive) and condition (stress, control) was used to examine the in-

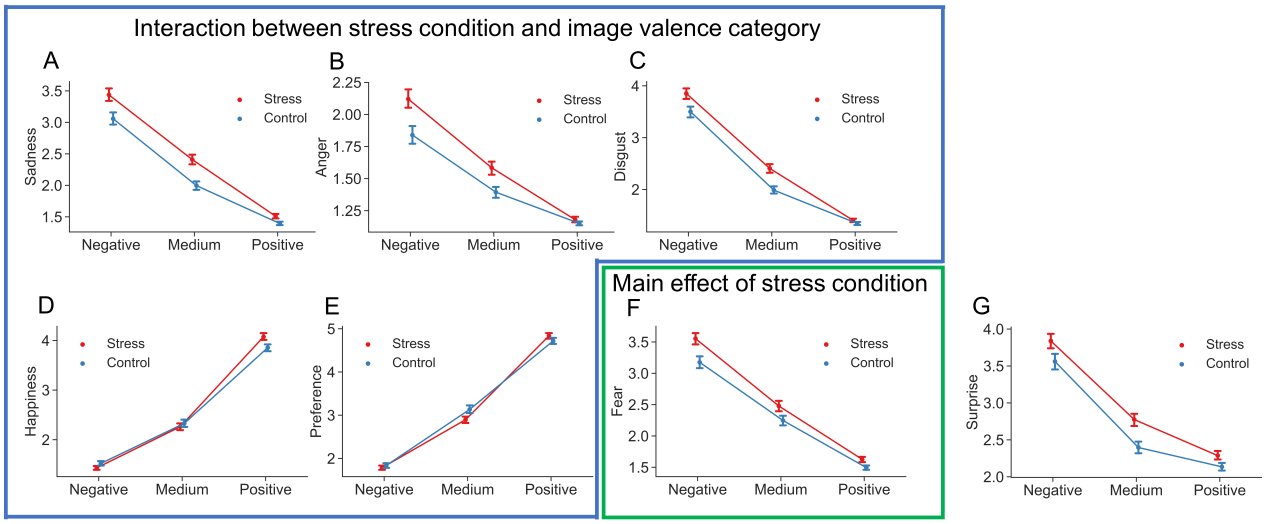

Figure 2.4: Subjective evaluation in the fMRI task. The plot of evaluation scores for valence assigned to images (negative, medium, positive) in stress (red) and control (blue) conditions. Sadness, anger, disgust, preference, and happiness showed significant interactions ($F(2,40) = 9.06$, $P < 0.001$; $F(2,40) = 2.82$, $P < 0.05$; $F(2,40) = 4.99$, $P < 0.01$; $F(2,40) = 3.81$, $P < 0.05$; $F(2,40) = 6.24$, $P < 0.01$, respectively, in two-way repeated measures ANOVA). Fear showed no interaction, but found the main effect of the condition ($F(2,20) = 7.89$, $P = 0.011$), but surprise showed no interaction and main effects. Error bars indicate the s.e.m.

teraction between valance (the effect of the image presented in the fMRI) and condition (the stress effect). When participants were looking at the image for three seconds, the right vmPFC (peak at Montreal Neurological Institute (MNI) x, y, z = 10, 40, − 8; F-value = 17.34; cluster size = 330 mm3; Fig. 2.5A,B) and left pre-supplementary motor area (SMA) (peak at x, y, z = − 6, − 28, 72; F-value = 10.91; cluster size = 162 mm3; Fig. 2.5A,B) showed the main effect of the valance (all result maps were tested with a cluster-defining threshold of $P < 0.001$ and cluster probability of $P < 0.05$, and were FWE- corrected).

In addition, using the brain clusters obtained from this analysis, we performed a correlation analysis between the brain region and psychological index (STAI scores and subjective ratings). The results showed a significant negative correla-

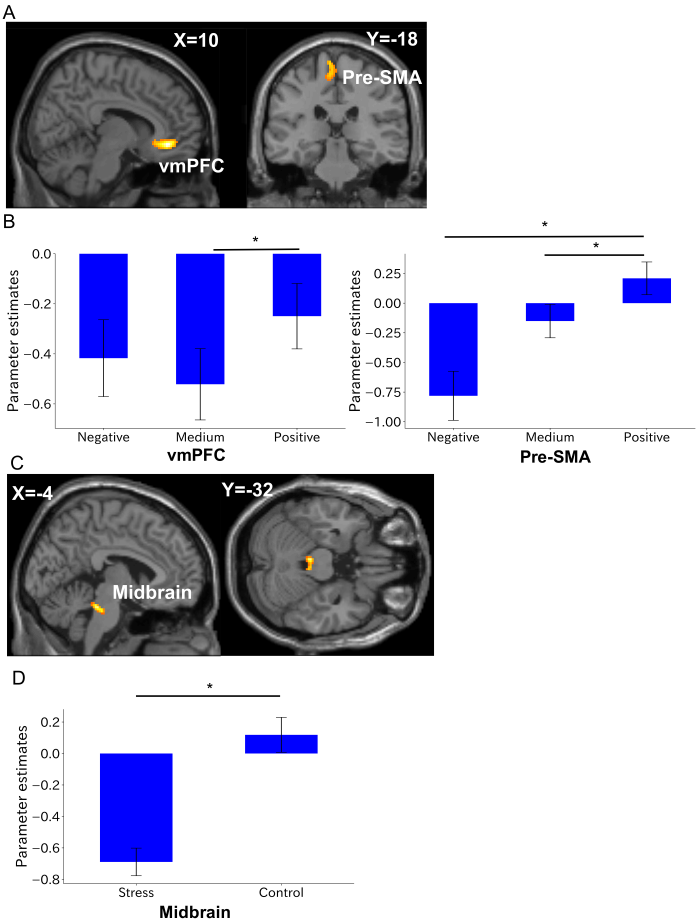

Figure 2.5: Whole-brain analysis. (A) The main effect of valence (negative, medium, positive) during the image display period. (B) Post-hoc analyses of parameter estimates of the image display period sorted by valence in the stress condition. (C) The main effect of condition (stress, control) during the evaluation period. (D) Post-hoc analyses of parameter estimates of the evaluation period sorted by valence in the stress condition. These results were obtained with a cluster-defining threshold of $P < 0.001$ and cluster probability of $P < 0.05$ and were FWE-corrected. *Survived Bonferroni correction for the number of elements in the condition. Clusters were overlayed on the T1-weighted template image (single_subj_T1.nii). Error bars represent s.e.m.

tion between the parameter estimate (mean regression coefficients of all trials in each condition) of vmPFC and STAI Y-2 ($r = -0.62$, $P = 0.0036$; Fig. 2.6A) before TSST in the stress condition but no significant correlation in the control condition ($r = -0.19$, $P = 0.42$; Fig. 2.6A). Furthermore, the parameter estimates in pre-SMA showed significant positive correlations with sadness ($r = 0.51$, $P = 0.019$; Fig. 2.6B left), fear ($r = 0.45$, $P = 0.039$; Fig. 2.6B middle), and disgust ($r = 0.42$, $P = 0.059$; Fig. 2.6B right) in the stress condition, although anger was only marginally significant ($r = 0.42$, $P = 0.059$; Fig. 2.6B right). However, no significant correlations were found in the control condition.
Next, The same ANOVA analysis was conducted while participants evaluated the presented images for 20 seconds. The results confirmed the main effect of stress in the left midbrain (peaks at x, y, z = −4, −32, −24; F-value = 25.59; cluster size = 145 mm3; Fig. 2.5C,D). All ANOVA results showed no interaction between valence and condition. Post-hoc analysis of the results comprised Bonferroni multiple corrections for the number of elements in the condition.

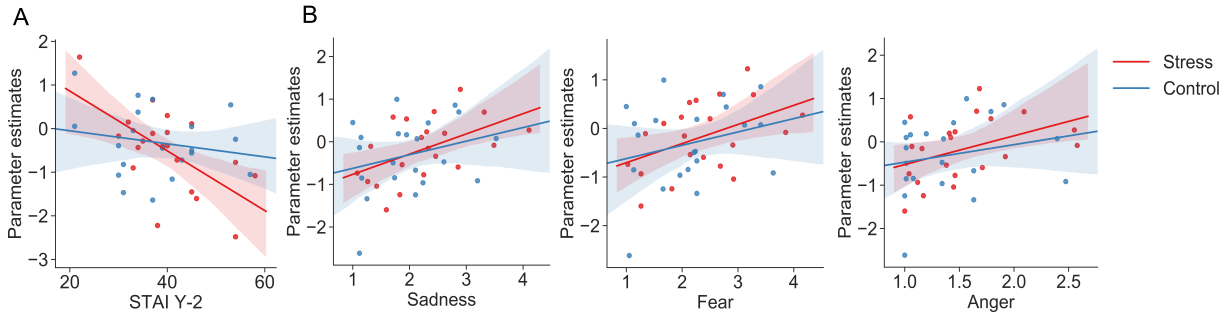

Figure 2.6: Correlation analysis in the vmPFC and pre-SMA. (A) Significant negative correlation between parameter estimates during the displayed-image period in the vmPFC and the STAI Y-2 (trait anxiety) measured before the TSST (− 40 min) ($r = -0.62$, $P = 0.0036$). (B) Significant positive correlation plot of parameter estimates during the image display period in the left pre-SMA and the subjective evaluation scores of sadness, fear and anger in the stress condition ($r = 0.51$, $P = 0.019$; $r = 0.45$, $P = 0.039$; $r = 0.42$, $P = 0.059$, respectively). Lines and colored areas are regression lines and 95% confidence intervals, respectively.

The detailed results of the whole-brain analysis are shown in Table.2.2(Cluster-defining threshold of P $<$ 0.001, cluster probability of P $<$ 0.05, FWE- corrected. MNI coordinates represent the peak voxels. Lat = laterality; L = left; R = right; B=Bilateral; BA=Brodmann's area; PFC=prefrontal cortex; vmPFC=ventromedial PFC; LC=locus coeruleus.)

Table 2.2: Brain areas showed the main effects of valence and stress on brain responses to the fMRI task after stress.

Phase	Main effects	Cluster size(mm^3)	Brain region	Lat	BA	MNI coordinates X Y Z	F value
Looking images for 3 sec	valence	330	vmPFC	B	11,32	10 40 -8	17.34
		162	SMA, pre-SMA	L	4,6	-6 -28 72	10.91
Evaluation displayed images for 20 sec	stress	145	Midbrain	L	-	-4 -32 -24	25.59

2.3.4 Functional connectivity for ROI-to-ROI analysis

To investigate the relationship between brain regions related to emotion ratings under stress, we performed a functional connectivity analysis using the brain regions, vmPFC, pre-SMA, and midbrain, as functional ROIs obtained by ANOVA (see "fMRI imaging result"). An ROI-to-ROI correlation analysis was performed to calculate the Z-transformed correlation coefficient to the average BOLD signal during target time-series signals in the ROI voxels. In functional connectivity between targets, we tested whether the contrast for stress and control conditions was significantly larger than 0. The ROI-to-ROI functional connectivity analysis showed significant functional connectivity between vmPFC and midbrain in the stress condition but not in the control condition(Fig.2.7A). Furthermore, we performed correlation analysis using functional connectivity between vmPFC and midbrain and changes in STAI Y-1 (state anxiety) before and after TSST. Unlike in the control condition (r = $-$ 0.1, P = 0.67; Fig. 2.7B), functional connectivity in the stress condition showed a significant negative correlation with changes in STAI Y-1 (r = $-$ 0.45, P = 0.048; Fig. 2.7A).

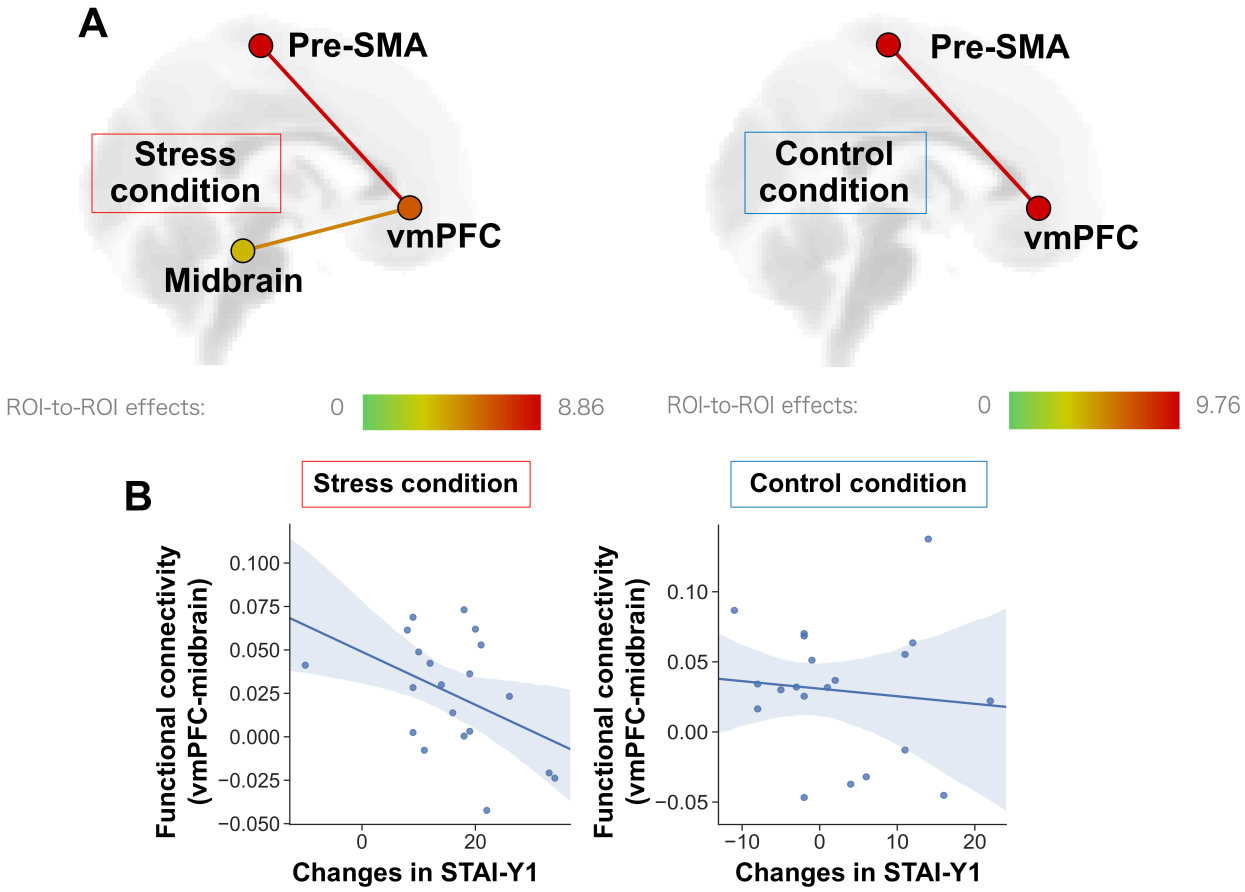

Figure 2.7: ROI-to-ROI analysis. (A) Functional connectivity between targeted areas (left, stress condition; right, control condition). Significant functional connectivity between the vmPFC and midbrain was observed only in the stress condition. The color bar of ROI-to-ROI effects indicates the F-value. (B) Correlation plot of functional connectivity between the vmPFC and midbrain against a change in the state anxiety in the stress condition ($r = -0.45$, $P = 0.048$) and the control condition ($r = -0.1$, $P = 0.67$). Lines and colored areas are the regression line and the 95% confidence interval, respectively. The images were created using the CONN software (ver.17.f, https://web.conn-toolbox.org).

2.4 Discussion

In an fMRI task after the acute social stress, we found that the prefrontal cortex activity was responsive to emotional stimuli and that activity differed according to image valence. In contrast, midbrain activity reflected the effects of stress as an emotional response. And then, vmPFC activity was significantly correlated with individual differences in trait anxiety. In addition, functional connectivity between vmPFC and the midbrain indicated individual differences due to anxiety over the stress response. This finding provides an essential mechanism for emotional regulation in the stress response and reflects the level of adaptation or modulation to the stressor.

According to the subjective evaluation performed with fMRI, we confirmed an interaction in the levels of stress effect and image valence, or a main effect of stress, mainly in negative affect. These results indicate that negative affect scores are different under stress than control. Previous studies showed that fear suppression is inhibited, and personal distress is exhibited under stressful conditions [46, 47]. In other words, less suppression of negative emotion indices than usual results in elevated values of negative emotions. Thus, it suggests that subjective evaluation scores in primarily negative emotions are overestimated by stress than healthy controls.

Consistent with the hypothesis, vmPFC activity under stress showed a significantly negative correlation with trait anxiety. This individual difference may reflect vulnerability to stress. Previous studies showed that stress enhances anxiety and harms emotional control [46,48,49] and that high trait anxiety contributes to individual differences in vulnerability to stress [50]. Thus, the result indicates the vulnerability of emotional regulation to stress. However, vmPFC has been detected as not stress effects but the main effect of valence. Although vmPFC regulates adverse effects by encoding emotional stimuli and subjective evaluation [23, 24, 51–53], vmPFC's emotion regulation is thought to be related to fear extinction and suppression. In other words, the vmPFC responds to the emotional stimulus and is not directly related to stress. Therefore, these results under stress suggest that the vmPFC expresses vulnerability due to negative emotion regulation when it responds to emotional stimuli.

Here, the pre-SMA showed a main effect of the valance. This result is consistent

with a meta-analysis in which the pre-SMA is associated with the execution of emotion regulation [54]. In addition, pre-SMA was positively correlated with subjective appraisal scores of negative affect in the stress condition. Prior research indicated that pre-SMA was associated with successful emotion regulation in limited negative contexts [55]. The pre-SMA was activated by reappraisal of the emotional evaluation of unpleasant images, and its activity was associated with successful reappraisal. Although participants in the experiments did not explicitly reappraise during emotion evaluation, these results suggest an effect of stress on pre-SMA functioning in cognitive appraisal.

Regarding emotional assessment, midbrain activity was reduced in the stress condition compared with the control condition. The midbrain is involved not only in homeostasis but also in emotion [56]. Previous studies showed that acute stress decreases limbic activity, and the midbrain is associated with stress initiation [57]. It supports the results and suggests that stress affects emotional responses, deactivates midbrain activity, and influences emotional regulation in homeostasis. More interestingly, the MNI coordinates of the peak value in the midbrain, detected as the main effect of stress, closely matched with that of the locus coeruleus in a recent meta-study [58]; the LC is the primary resource of noradrenaline and projects to various brain regions, including the prefrontal cortex [59]. LC activity is independent of valence. It is associated with the acquisition of emotional input, the storage of emotional memories, and the maintenance of cognitive processing [60,61]. In addition, reduced LC responses suggest enhanced resistance, consistent with midbrain results from the whole-brain analyses [62]. One interpretation is that the portion of the midbrain detected as the main effect of stress is working with other brain regions to mediate psychological responses to stress. However, the LC was difficult to detect using standard fMRI methods, and precise peak coordinates could not be identified [63].

Finally, functional connectivity between vmPFC and midbrain under stress conditions showed individual differences in state anxiety. State anxiety reflects high-stress [64], supporting our results. In addition, vmPFC coupling with the limbic system and brainstem is important for emotion regulation, and stress resilience [31, 65]. Indeed, these circuits contribute to negative emotion processing, motivation for action, and fear of extinction [66–68]. Recent human MRS

studies suggest that these circuits are related to the neuroscientific function of the vmPFC in emotion processing, and local GABA levels in the vmPFC were associated with the functional connectivity between the vmPFC and amygdala with personal anxiety [27–29]. However, our findings failed to detect the effects of valence and stress on limbic systems such as the amygdala, which is specifically involved in emotion processing. Previous studies showed that functional connectivity between the vmPFC and the amygdala is associated with negative emotion [20,66]. In addition, brain regions associated with negative emotion and stress can be overlapped. Though the amygdala is associated with emotional processing, it is strongly responsive to emotional processing, stimulated by facial expressions [69]. The images used in the experiment included a variety of categories, and the valence scores of the stimuli were balanced between stress and control conditions. It may explain why no amygdala activity was observed in our experiment.

The finding that functional coupling between the vmPFC and the midbrain reflected individual differences in emotion regulation in the stress response might provide new insights into treatments for controlling stress vulnerability factors and mental disorders such as major depressive disorder. From an emotion regulation perspective, some psychiatric disorders are characterized by vulnerabilities in emotion regulation, and emotion regulation is important in mental health [70,71]. Our findings may help to measure stress resilience in negative emotion regulation. In psychiatric disorders, recent animal studies of deep brain stimulation (DBS) indicated that vmPFC under DBS affects LCs to produce antidepressant-like effects [72]. In addition, functional connectivity real-time neurofeedback has been applied to some psychiatric disorders [73,74]. Future studies should establish new biomarkers for treating specific psychiatric disorders through neurofeedback and DBS.

In addition, various experimental paradigms and findings exist in stress and emotion regulation. For example, although not introduced in this study, it has been pointed out that there are three types of strategies that promote emotion regulation: reappraisal, suppression, and distraction [75]. These emotion regulation strategies require cognitive control systems and working memory by brain regions related to executive control [9,76,77]. However, stress is known to impair

working memory, which is needed to facilitate emotion regulation [78, 79]. Prior research has shown that stress-induced working memory impairment prevents sophisticated strategies that require working memory (model-based). However, stress does not affect simple, principled strategies (model-free) [77]. And then, theta burst stimulation (TBS) of the Dorsolateral Prefrontal Cortex (dlPFC), which is associated with working memory, results in individual differences in the strategies. In addition, it depends on working memory capacity [76]. Although our fMRI study revealed a relationship between stress and emotion regulation, the relationship between stress and strategies for emotion regulation is not clear. Therefore, further research is needed to determine the extent to which cognitive strategy for emotional regulation is robust against stress.

Several limitations are imposed on the generalizability of our results. First, subjects were asked to participate in an experiment in the stress and control conditions. As a result, a framing effect occurred in this experiment [80]. However, participants were asked to participate in the control condition at least two days after being acutely stressed by the stress test. In terms of brain networks and neurosecretion in response to stress, it has been noted that recovery from acute stress is complete within several hours [81]. Therefore, we do not believe that the effects of stress inflicted in the stress condition will impact the control condition. However, we could not eliminate the uncertainty as to whether or not framing effects were occurring. Thus, there is a need to conduct future experiments with participants assigned in random order in the stress and control conditions. Another limitation is only male subjects participated in the investigation of this study. Women's stress response would be replaced by menstrual cycles, and oral contraceptive use [38]. Previous studies measuring stress biomarkers indicated that sex differences should be careful. For example, in the TSST study testing saliva as a biomarker, 12 of 35 studies were reviewed in male-only participants [82]. And then, the activity of PFC is associated with emotion regulation [83], and that of emotion regulation differed between male and female rats [84]. In summary, gender differences may be responsible for specific emotion regulation in the stress response. Thus, the generalizability of our findings to women remains the problem.

3 Two modes in locus coeruleus have essential roles for stimulus encoding

3.1 Background

Neurons and neural networks function as real-world system that detects or identifies signals from outside. This system allows people to flexibly adapt to sensory processing, attention, and unexpected events by applying modifications at the cognitive level when information comes in from the five senses.

Locus coeruleus (LC), the primary source of noradrenaline, regulates cognitive functions, including attention and memory processing, by modulating neural activity in cortical areas [60, 61, 85, 86]. The neural activity of LC is projected to many brain regions, and the role is specific to the brain region [87–89]. Thus, although various previous research shows the relationship between LC and other brain regions, the detailed mechanism of LC as an intrinsic modulator is unclear.

From a neuronal perspective, there are typically two distinct firing modes as a modulator of the LC: tonic and phasic firing [90]. Tonic firing is characterized by sustained, spontaneous firing. In contrast, phasic firing is characterized by transient, small numbers or firing bursts. The example of the tonic and the phasic signal is shown in Fig.3.1.

The coexistence of these two firing characteristics has been found to regulate various neural systems and coordinate different functions at the brain network level [91,92]. For example, phasic plays an essential role in salient encoding stimuli and facilitates the encoding of salient stimuli in sensory neurons [93]. And then, phasic and tonics encode the exact opposite valence and coordinate differently for

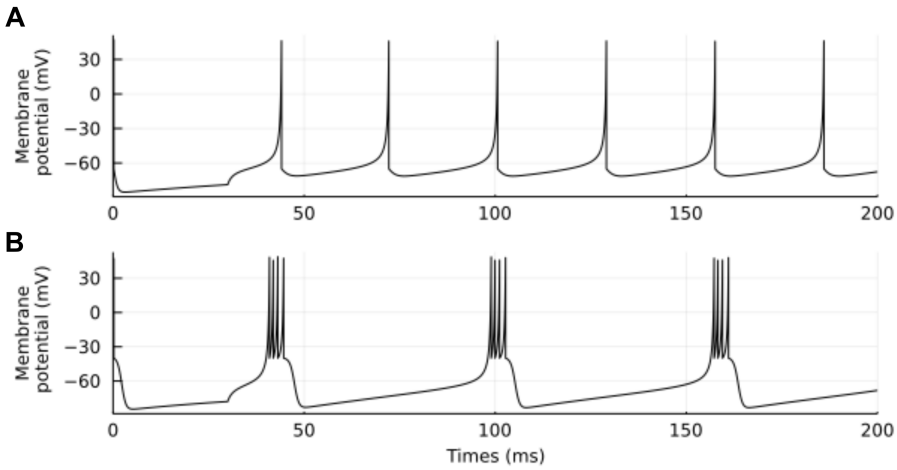

Figure 3.1: Examples of membrane potential to tonic and phasic signal. (A) Tonic signal. (B) Phasic burst signal.

arousal coordination, indicating that LC activity patterns affect both networks and behave differently [94, 95]. Furthermore, previous studies showed that the external cognitive load alters these firing rate balances. One of the most famous cognitive loads closely related to the LC is stress, which causes the phasic to prioritize the tonic firing when stress occurs [96–98]. Under appropriate stress, tonic firing promotes cognitive flexibility and arousal. However, excessive tonic firing under heavy stress can lead to hypervigilance and distractibility. Thus, dysfunction of the phasic-tonic balance can lead to various mental disorders [99, 100].

In addition, some simulation studies in LC have been validated at the neuronal level and have examined performance in cognition and interactions between noradrenergic neurons [59, 101]. Two firing properties of the LC have also been tested in a rewarding task related to exploration/exploitation of reinforcement learning [102]. This study suggests that state-action prediction errors reflect the phasic/tonic LC activity and that these firing properties made updates. Furthermore, the authors propose the hypothesis that such prediction errors are mediated by cortical-LC coupling and that LC to cortical inputs modulate learning rate updating in the ACC. In addition, some previous studies have tested the modulatory effect of the LC in a multilayer model [103]. The results show that

the single-layer model did not improve rewards, whereas extending the model to multiple layers resulted in improved gains.

Although the role of LC in brain regions and their impact on cognition and behavior at the neuronal level has been investigated, there are few examples of studies simulating the function of LC at the neural population level. Likewise, although the role of phasic/tonic signals generated by the LC and their impact on cognition and behavior at the neuronal level have been investigated, there are few examples of studies simulating LC function at the neural population level. It is generally known that most sensory information is transmitted to the cortex via the thalamus [104]. However, these processes are propagated in a multi-layered neural network model. Prior research has shown that neural responses to sensory processing depend on external inputs and internal network variables defined as a network of populations [105]. It has also been suggested that the presence of recurrent feedback is necessary to form ongoing activity [106–108]. The influence of these internal network variables and feedback is unique to neural population networks, and quick corrections in recognizing stimulus changes should be better in a population than in a single neuron [109–111]. Thus, modeling neural responses to sensory processing would require building a multi-layered model with random synaptic connections and feedback structures. It has also been noted that phasic/tonic in the LC is associated with attention and arousal [59,94]. However, since sensory information is encoded in the prefrontal cortex, it is assumed to function as a modifier rather than retaining cognitive information. Taken together, to model the phasic/tonic role of the LC in this study, it is crucial to represent the regulatory function of the LC as a population in a way that does not disrupt its molecular structure. We developed a multi-layered feed-forward neural network model that can incorporate signals generated by the LC as an internal model.

In this model, we hypothesized two signals as modulators. The first is a homogeneous signal, a population of multiple tonic firing. The second is an inhomogeneous signal, a population of multiple phasic firing. By combining these signals with a feed-forward multilayer network with intra-layer random connections, we investigated the role of the modulator at the neural population level.

The results showed that the homogeneous mode detected strong spike coher-

ence. It indicated that the linear transformation of the input signal was converted into spike coherence, and the differential coding of the input was encoded. On the other hand, the inhomogeneous mode could not encode differential coding compared to the homogeneous mode. And then, frequency dependency enhancement of the differential signal was detected in the homogeneous mode, but not inhomogeneous mode. In addition, it become more dominant from inhomogeneous mode (phasic) to homogeneous mode (tonic), and the transmission rate increases continuously. Therefore, it suggests that the homogeneous mode can be contributed to the enhancement for encoding inputs, but the inhomogeneous mode to suppression of a spike coherence prevented excessive cognition influence.

3.2 Materials and Methods

3.2.1 Network Architecture

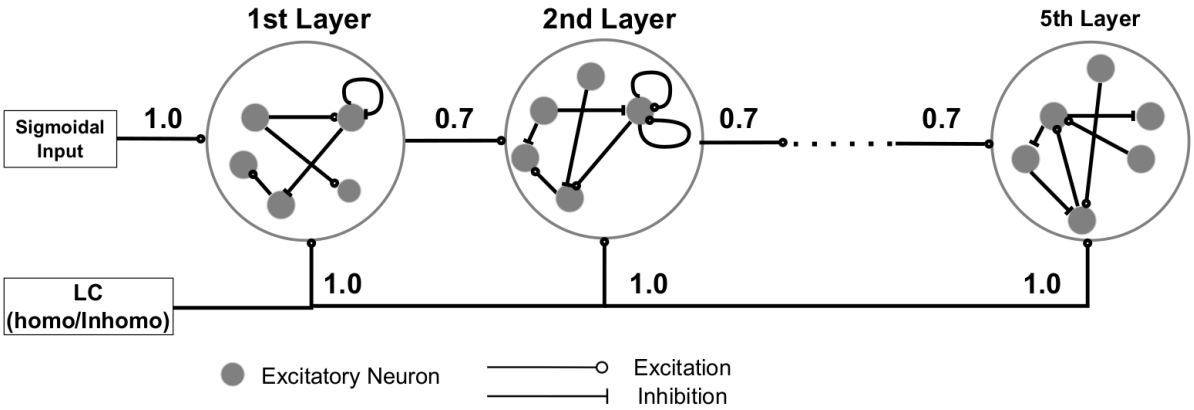

Figure 3.2: Five-layer's feed-forward network model with the intra-layer random connection.

A network architecture was developed following the previous research [112]. The model is shown in Fig.3.2. This model comprises a five-layer feed-forward network, with 100 excitatory neurons in each layer. Each layer has random excitatory and inhibitory connections. The number of excitatory synaptic connections in each layer was set at 60, and the number of inhibitory synaptic connections at 30. The network architecture was simulated 100 times, with each simulation providing a different intra-layer connection. Excitatory synaptic connections between the layers are transmitted with a probability of 0.7.

Two kinds of inputs are projected into the first layer. The first input is frequency changes like a step function and generates a spike in a sinusoidal manner. The sinusoidal input is illustrated in Fig.3.3. The input is composed of three parameters: change interval $W(ms)$, base frequency $f_{ext}(Hz)$, and frequency change $f_{diff}(Hz)$. All the intermediate time of stimulus change point was set at 800 ms. There are two motivations for simulating the response to sinusoidal inputs. First, it is possible to reconstruct the response of a network to an arbitrary time-dependent input. The second is that oscillations have been observed in many central nervous system brain regions and are a common input to synap-

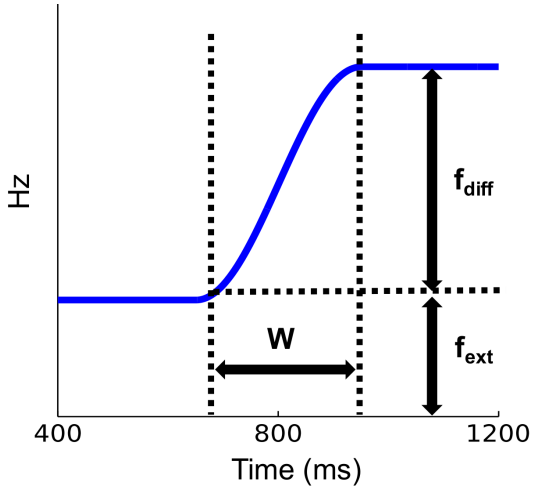

Figure 3.3: The signal frequency changes in a sinusoidal manner.

tic structures. In other words, a dynamic frequency change was modeled by the signal change of natural stimuli. The second input is homogeneous or inhomogeneous modes in the LC model. LC model's inputs are projected into all layers, and the generated inputs are different from each layer. The detail of the LC model is described in the next section.

3.2.2 LC model

In the LC model, we used two modes as another input projected into the layers. The first signal is the homogeneous mode. This mode was generated following to homogeneous Poisson process, so the firing rate lambda is constant [113]. On the other hand, the inhomogeneous mode was developed following to Ornstein-Uhlenbeck process [114]. The update formula is followed by the Euler-Maruyama method and is shown as below,

$$d\lambda(t) = \theta \cdot (\mu - \lambda_t)dt + \sigma W(t) \qquad (\lambda_0 = \lambda_{init}) \tag{3.1}$$

where theta is set to 0.1, and μ is equal to σ and λ_{init}. The firing rate of the homogeneous mode and the expected value(μ) of inhomogeneous mode (i.e., variance σ and initial value λ_{init}) will be denoted uniformly as $f_{int}(Hz)$. Fig.3.4 is an overview of our hypothesis, and right figure shows example of each mode and

generates five firing patterns as a population.

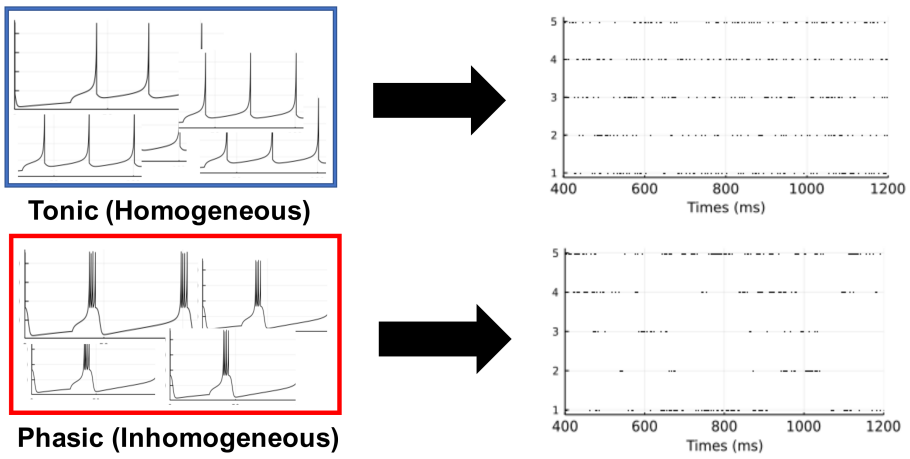

Figure 3.4: Overview of our hypothesis to homogeneous and inhomogeneous mode. Homogeneous mode is represented as an overlap of a tonic signal. On the other hand, the inhomogeneous mode is expressed as an overlap of a phasic burst. The right figure shows five samples of generated firing patterns based on our hypothesis.

Taken together, in the absence of any information, a constant frequency ($f_{ext} + f_{int}$) is propagated. However, all signal information is represented by a frequency change (f_{diff}).

3.2.3 Neuron model

In our experiment, the Hodgkin-Huxley model was used as a neuron model [115].

$$C_m \frac{dV}{dt} = - \sum_{j=Na,K,l} g_j(V - V_j) + I_{syn}, \tag{3.2}$$

where $C_m (= 1.0(\mu F/cm^2))$ is the membrane capacitance, $g_{Na} (= 120.0m^3h(mS/cm^2))$ is sodium conductance, $g_k (= 36.0n^4(mS/cm^2))$ is potassium conductance. $g_l (= 0.3(mS/cm^2))$ is leak conductance. In the Hodgkin-Huxley model, we used four variables; V, m, h, n. And then, m, h, n obey the differential equation as below,

$$\frac{dx}{dt} = (\alpha_x(V)(1 - x) - \beta_x(V)x) \cdot 3^{((T-6.3)/10)}, \tag{3.3}$$

where T is temperature, human cortical nerves are highly nonlinear at high temperatures. The default temperature setting slows down the differentiation, making it challenging to detect firing successfully. Therefore, the temperature in this study was set to 15 degrees Celsius [116]. The Hodgkin Huxley model set the temperature at 6.3 degrees Celsius by default, modeled after squid axons. Reversal potentials(mV) are as follows: $V_{Na} = 50.0 - E_r, V_K = -77.0 - E_r, V_l = 54.4 - E_r$, where $E_r(= -65.0(mV))$ is the resting potential. $\alpha(V), \beta(V)$ is different from variables; m, h, n. These variables is followed subsequent six formula as below,

$$\alpha_m(V) = \frac{0.1(25-V)}{\exp[(25-V)/10]-1}, \qquad \beta_m(V) = 4\exp(-V/18)$$
$$\alpha_h(V) = 0.07\exp(-V/20), \qquad \beta_h(V) = \frac{1}{\exp[(30-V)/10]+1}$$
$$\alpha_n(V) = \frac{0.01(10-V)}{\exp[(10-V)/10]-1}, \qquad \beta_n(V) = 0.125\exp(-V/80)$$

3.2.4 Synapse model

In the synaptic event, we define the conductance model as an α function [117,118]:

$$g^i_{syn}(t) = r_i \cdot \frac{g_{peak} \cdot (t - t_i)}{t_{peak} \cdot S} \exp^{1-(t-t_i)/t_{peak}} \tag{3.4}$$

where r_i denotes synaptic efficiency, S is a surface area ($= 20\mu m$), $t_i(ms)$ is firing time, and $t_{peak}(ms)$ is time constant at which the conductance reaches its peak value of $g_{peak}/S(mS/cm^2)$. Time constant(t_{peak}) was set to 2.0 and 5.0 (ms) for excitatory and inhibitory synaptic connections. Each excitatory synaptic connection defines the g_{peak}. For each simulation, g_{peak} were sampled from a Gaussian distribution $N(1.0, 0.5)$, in excitatory connection and inhibitory synapse connection were fixed at $g_{peak} = 5$. And then, synaptic efficiency was multiplied by 0.5 in the case of a spike event and recovered with a time constant of $500ms$ to represent synaptic depression. The synapse efficacy of inhibitory connection was set to 1. It is because the inhibitory connections do not need to consider synaptic depression. The firing in a pre-synaptic neuron does not immediately propagate into a post-synaptic neuron. So synaptic delay was set to 2.0 milliseconds in the excitatory connections. However, those inhibitory synaptic connections were followed by the exponential distribution: $\exp(-t/500) + 5.0(ms)$. The delay

distribution models the distribution of times necessary for a gap junction network to transmit spikes.

3.2.5 Measurement of the histogram and spike coherence

In the simulation, one hundred run paths were performed. And then, peristimulus time histo- grams (PSTHs) were generated by binning spike rates into 5 ms bins.

$$h(t) = \frac{1}{100}\sum_{i=1}^{100} h_i(t) \tag{3.5}$$

where $h_i(t)$ is the number of spikes in the ith path at time bin at t(bin width $\delta t = 5ms$).

In addition, the spike coherence in the fifth layer was calculated to examine the correlation or relationship of the various stimulus types. It was then compared in a homogeneous or inhomogeneous mode. Spike coherenceX_p is defined as follows.

$$X_p = max_{t\in 700\sim 900ms} X(t), \tag{3.6}$$

$$X(t) = \frac{x(t-\delta t) + x(t) + x(t+\delta t)}{3}, \tag{3.7}$$

$$x(t) = h(t) - < h(t) >_{t\in 900\sim 1100ms}, \tag{3.8}$$

First, the number of spontaneous firings x(t) was smoothed by subtracting the post-firing baseline from the histogram. The brackets $< h(t) >$ means the average of the target interval. Next, to suppress artifacts that arise when dividing the time into bins, X(t) is defined as the average of the sum of three continuous x(t). Then, extracting the maximum value of X(t), the intensity information that retains the most differential information of sinusoidal input, is extracted.

3.3 Results

3.3.1 Histogram results

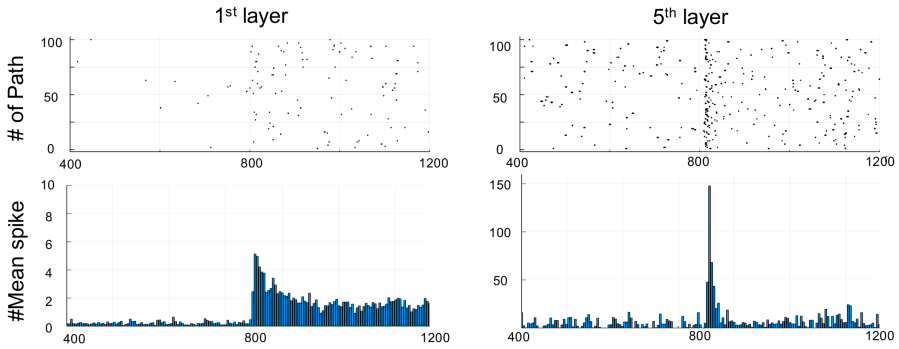

Figure 3.5: Population responses of the homogeneous mode in the first and fifth layers. Raster plots show spikes series of a particular neuron (index 0) in 100 simulation runs. The histogram indicates the number of spikes in the 100 simulation runs at a time bin of 5 ms. The parameters of the two inputs was set to $f_{ext} = 100Hz, f_{diff} = 200Hz, W = 10ms, f_{int} = 100Hz$.

Using these models and performing in the network architecture, we found that the population response in the fifth layer encoded the differential coding. To the same input, Fig.3.5 shows that a soft edge was detected in the first layer, but the strong spike coherence differential information emerged in the fifth layer. And then, The histograms were compared between the homogeneous and inhomogeneous mode. Fig.3.6 indicates that the first layer is nearly the same in both modes. However, in the fifth layer, the homogeneous mode in locus coeruleus showed better performance than the inhomogeneous mode.

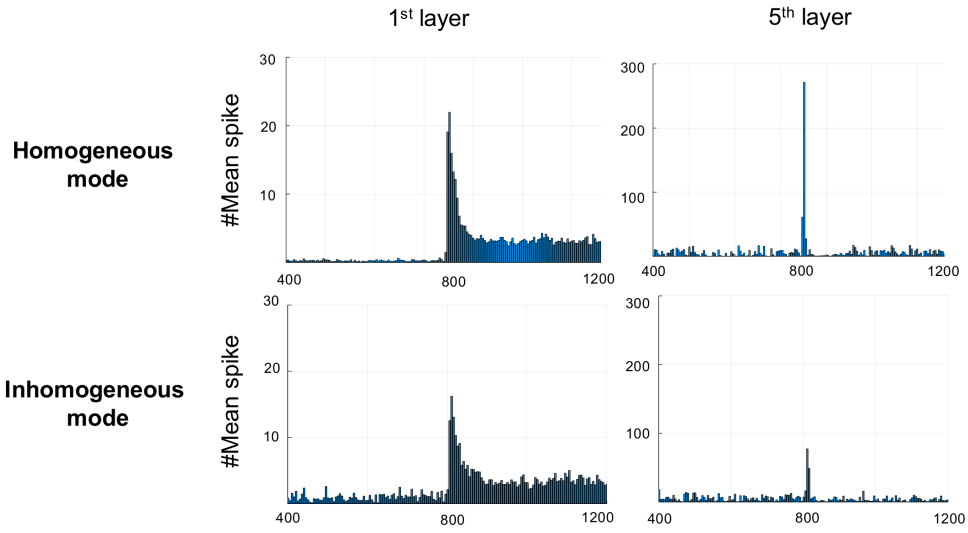

Figure 3.6: Population responses of the homogeneous and inhomogeneous mode in the first and fifth layers. The histogram indicates the number of spikes in the 100 simulation runs at a time bin of 5 ms. The parameters of the two inputs was set to $f_{ext} = 100Hz, f_{diff} = 500Hz, W = 10ms, f_{int} = 100Hz$.

3.3.2 Spike Coherence results

In Fig.3.7, a negative correlation emerged, with firing coherence decreasing as the frequency change's interval became large. On the other hand, spike coherence showed a positive correlation as the frequency increased. In the case of a homogeneous mode, the spike coherence was more sensitive to stimulus than in the inhomogeneous case, and the differential information of the input was encoded better. However, the effect was small in the inhomogeneous process, indicating that spike coherence was suppressed.

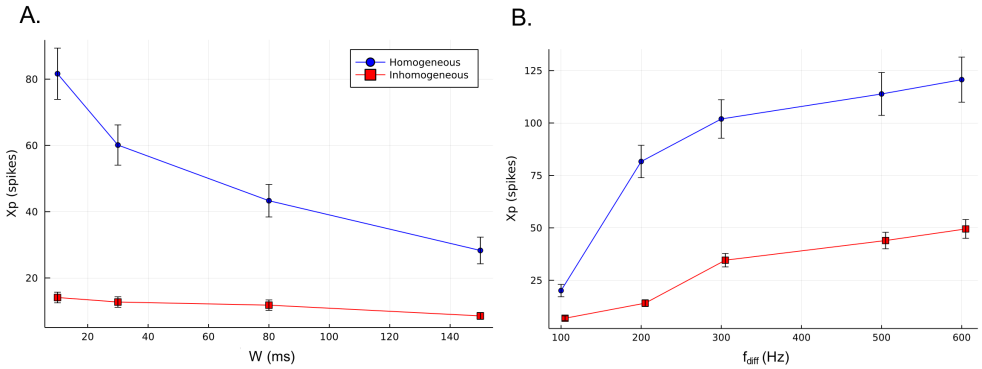

Figure 3.7: (A) Homogeneous and inhomogeneous mode with the change interval W ($f_{int} = f_{ext} = 100Hz, f_{diff} = 200Hz$). (B) Homogeneous and inhomogeneous mode with the change frequency f_{diff} ($f_{int} = f_{ext} = 100Hz, W = 10ms$). Error bars indicate s.e.m.

3.3.3 Noise enhancement

And then, we examined whether the frequency of the modes has the optimal sensitivity of a nonlinear system (Fig.3.8). As a result, in the case of the homogeneous modes, it exists at a certain intensity, and the differential detection is optimized in the fifth layer. On the other hand, the inhomogeneous mode only reduced spike coherence and depended on the frequency. It shows stochastic resonance in the homogeneous mode.

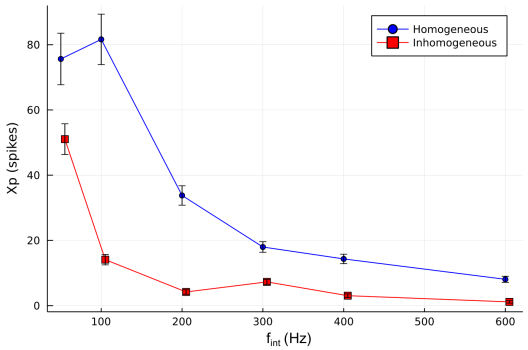

Figure 3.8: Enhancement for the LC models input frequency. The parameters of the stimulus input was set to $f_{ext} = 100Hz, f_{diff} = 200Hz, W = 10ms$. Error bars indicate s.e.m.

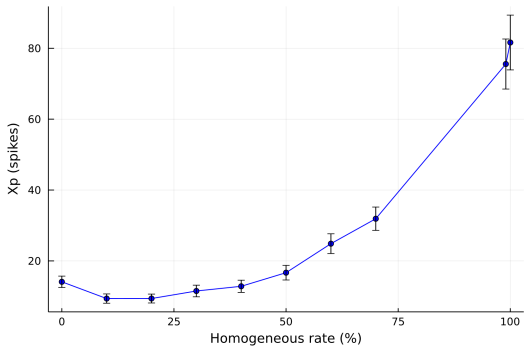

Figure 3.9: Enhancement for the LC models input frequency. Note that f_{int} indicates the firing rate and expected value in the homogeneous and inhomogeneous modes. Error bars indicate s.e.m.

3.3.4 The rate change in homogeneous and inhomogeneous modes

We assumed that all the homogeneous or inhomogeneous modes were projected into all neurons. Therefore, we must consider the rate of the two modes projected into the excitatory neurons. In Fig.3.9, we changed the rate of the homogeneous and inhomogeneous modes projected into all neurons in each layer. The rate is the same and fixed in each layer, and the rating formula is written below.

$$inhomogeneous \times (1 - \alpha) + homogeneous \times \alpha \tag{3.9}$$

As a result, we found more dominant from inhomogeneous mode to homogeneous mode, and the transmission rate increases continuously.

3.4 Discussion

To model the firing pattern mechanism of LC, we separated the homogeneous and inhomogeneous modes to combine feed-forward neural networks. As a result, the homogeneous mode encoded differential information. However, the inhomogeneous mode does not encode compared to the homogeneous mode. And then, the inhomogeneous mode only reduced spike coherence depending on the frequency. The more homogeneous mode continuously increased the spike coherence. Our findings reveal that dynamic balance can be existed and plays the inverse role between the homogeneous and inhomogeneous modes in LC.

In terms of the histogram, the sharp histogram was detected at the change point of input's frequency in the fifth layer compared to the first layer. The result supports the simulation study of LC that a gain improves for the transition from layer to layer [103]. It also supports the synfire chain hypothesis, which synchronously propagates as a cascade from layer to layer [119]. It suggests that the temporal variation of the spike series is composed of synchronously bearing coincident spikes, which can be detected to varying degrees but independently of the firing characteristics.

The homogeneous mode showed better differential coding performance than the inhomogeneous mode. The tonic firing increases the gain of the network indiscriminately and makes it more responsive to any stimulus [96, 120]. Thus, it is suggested that the homogeneous mode, expressed as a superposition of tonic firings, facilitates the detection of differential information.

On the other hand, the spike coherence of the inhomogeneous mode was lower than that of the homogeneous mode, which may be due to fluctuations' influence. Prior studies have shown that population fluctuations regulate signal synchronization [121]. Therefore, due to the large fluctuations, spike coherence could not be detected well in inhomogeneous mode, which is a collection of burst firings. Furthermore, it has been pointed out that phasic firing is necessary to release noradrenaline, reduce ASR activity, and promote anti-inflammatory effects [122, 123]. And then, according to network reset theory, phasic bursts may suppress or reset activity in the target network [124]. Therefore, the inhomogeneous mode may play an essential role in mental disorders by suppressing the excessive spike coherence to interrupt a lousy cognition. And then, the results showed that the

histogram of the first layer is not different from that of the homogeneous mode but is very different in the case of the fifth layer. It indicates that the suppression effect of the inhomogeneous mode is critical for propagating from layer to layer.

Here, in the case of the homogeneous modes, it exists at a certain intensity, and the differential detection is optimized in the fifth layer. On the other hand, the inhomogeneous mode only reduced spike coherence and depended on the frequency. Previous research indicated that tonic firing exhibits an inverted U-shaped in detection, supporting our present results [125]. For example, bursts of noradrenergic overexcitation cause behavior observed in people with neuropsychiatric disorders, and high-frequency stimulation in LC results in reversible behavioral arrests [94]. Thus, the homogeneous mode, which is a superposition of tonic firings, suggests an optimal frequency useful for stochastic resonance.

Finally, the transmission rate increases continuously from the inhomogeneous mode to the homogeneous mode. It supports previous studies in which tonic and phasic firing encoded the opposite information. In the present case, the homogeneous mode may increase differential information detection. In contrast, the inhomogeneous mode may be involved in suppression. Furthermore, prior studies have indicated that the LC signals emitted to control arousal are specific and task-dependent [126]. It has also been noted that the noradrenergic LC is highly plasticity and substantially changes brain state modulation [127]. These results show that LC can continuously regulate the signal by switching between homogeneous and inhomogeneous modes flexibly.

Our findings may also be helpful in the treatment of mental disorders. For example, variations in LC activity patterns are responsible for individual differences in the development of Alzheimer's disease in humans [128]. It supports the finding that spike coherence is continuously regulated by the ratio of the homogeneous and inhomogeneous modes. The individual differences in this regulation may be related to psychosis. Another example is that local cooling of epileptic brain regions consistently suppresses epileptic seizures [129]. This previous research indicated that temperature dependence is essential in determining whether suppression or termination of epileptic discharges in response to cooling can be achieved. In addition, when spikes are converted in higher-order regions, such as the frontal lobe, the frequency is low, and burst firings are unlikely to occur.

Suppose epilepsy occurs as bursts of tonic firing. In that case, the inhomogeneous mode might provide another solution to suppress epilepsy and contributes to the internal suppression of epileptic discharges as a modulator. Furthermore, our results could be helpful in treating stress, which is closely related to noradrenaline [98]. It has been noted that noradrenaline functions specifically in brain regions and tasks to control arousal [126]. Our results suggest that the inhomogeneous mode inhibits and regulates stress-induced hyper-recognition.

In limitation, the number of excitatory and inhibitory connections was fixed in each layer. So we can not consider the effect of the rate of these connections. Specifically, excitatory synaptic connection contributes to synaptic depression. The synaptic depression helps suppress the burst firing effect in the inhomogeneous mode. So further study is needed to estimate the influence between the excitatory and inhibitory synaptic connection rate. And then, in the simulation study, we implicitly focused on not valence but arousal; nevertheless, we focused on emotional valence in the fMRI study. The locus coeruleus-norepinephrine (LC-NE) system generally mediates arousal [96]. However, a recent previous study showed valence encoding of LC's stimulation was provided [95]. And then, tonic stimulation encoded aversion and phasic stimuli in LC encoded preference [92]. Therefore, further research is needed to provide general findings combining valence and arousal in the cognitive aspect.

4 General Discussion

This thesis examined two approaches to demonstrate stress mechanisms: a macroscopic approach at the brain region and a microscopic approach at the neuronal level. This thesis presents two lines of research on this topic.

In the first study, to demonstrate the adaptive response of the brain mechanism under acute stress, we used fMRI to analyze brain activity in individuals for performing emotional evaluation tasks and assessing the intensity of their emotions after acute social stress. As a result, the ventromedial prefrontal cortex (vmPFC) and pre-SMA responded to the emotional image's valence, but the midbrain during evaluation as stress effect. In addition, prefrontal regions such as vmPFC and pre-SMA showed individual differences in emotion regulation such as subjective appraisal and trait anxiety under acute social stress conditions. Functional connectivity between the vmPFC and the locus coeruleus (LC) was negatively correlated with acute social stress effects. These results suggest that the function of networks, including the vmPFC in emotion regulation, is influenced by the extent of an individual's stress response.

In the second study, to model the LC firing mechanism, we assumed two signals; homogeneous and inhomogeneous modes. The homogeneous mode is expressed as an overlap of tonic firing. On the other hand, the Inhomogeneous mode is represented as an overlap of phasic firing. Combining these modes into a feedforward network model as modulatory input, we found that a homogeneous mode of LC represented stimulus change well. This homogeneous mode can be applied to quick responses. Moreover, the inhomogeneous mode was inapplicable because of the fluctuation of the mode. However, inhomogeneous modes can contribute to mental disorders by suppressing excessive spike coherence and modulating

harmful cognitive effects. This effect can be continuously controlled by changing the ratio of the homogeneous and inhomogeneous modes. It suggests that the LC flexibly switches between homogeneous and inhomogeneous modes expressed as phasic and tonic firing populations to adjust the signal dynamically.

Our research mainly identifies the importance of activity and functional connectivity, including vmPFC, as a relationship between brain regions contributing to the individual difference in stress-induced cognition from the fMRI study. Next, we developed a bio math model to investigate the factors contributing to the individual differences in stress found in an fMRI study. Specifically, focusing on two signal properties at locus coeruleus, we hypothesized two signal modes and conducted the simulation study. The results suggest that the two signals play specific roles. In addition, by changing the ratio of these two modes, the model allows flexible regulation of the differential coding, and there is an optimal mode frequency in the homogeneous mode. We hypothesized that the strength of these proportions and frequencies might influence frontal lobe regulation, resulting in individual differences in cognitive processing related to our anxiety and attention to stress. These results may apply to the different roles of the modes in clinical experiments to alleviate acute stress by, for example, conducting neurofeedback experiments related to the vmPFC and the midbrain. Also, by taking advantage of the characteristics of the two LC modes, we may allow for analysis of the differences in the roles of the two signals in the same time series as explanatory variables.

Here we propose a hypothesis that summarizes the results of these two studies. The vmPFC found in fMRI studies has a role in fear recovery [130] and consists of areas 24, 25, 32, 11, and 10 in the Broadmann map [131]. In particular, the regions of peak value in the vmPFC that emerged from the whole-brain analysis of our fMRI study included BA11 and BA32, so they contained OFC and dorsal ACC. The previous research shows that OFC and dACC in the vmPFC have monitored LC to generate patterns of LC activity to optimize the utilities in the time series [96, 132]. The results correspond with neural projection, and some previous studies show that LC is projected from vmPFC [133, 134]. In addition,

some previous research indicates a negative correlation between the vmPFC and LC [135, 136]. It is associated with our fMRI study that the negative functional connectivity between vmPFC and LC in the case of worse change of state anxiety due to stress. Therefore, vmPFC regulates LC downstream, which might lead to lower activity in the vmPFC (OFC and dorsal ACC) and higher activity in the midbrain (LC) in the case of large changes in state anxiety to stress are significant. And then, it suggests that when stress coping is not successful, the homogeneous mode may become dominant, and overall LC activity would increase.

However, it was not possible to investigate how the effects of stress affect the cognitive at neural levels. There are several possible ways to examine these relationships. The first approach would be to test whether stress is modulated by stimulating neurons by using the two signal modes of LC at different intensities and rates under stress. This approach may lead to a better understanding of the effects of stress at the neural level. The second possible method would be to examine the degree of regulation in the prefrontal regions by investigating the effects of the two signal modes of the LC proposed in the hypothesis on noradrenaline secretion by comparing stress or not. It might allow us to understand how much these two modes can release noradrenaline and how stress affects our cognition from neural levels.

5 Supplementary Information

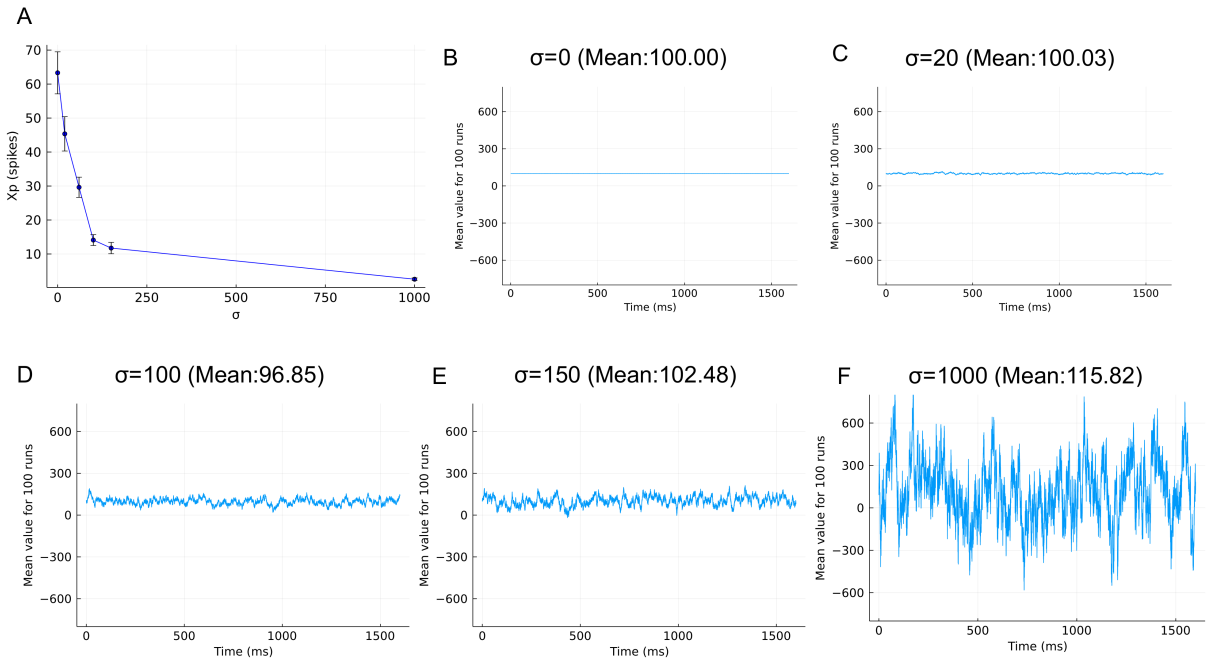

Figure 5.1: (A) Spike coherence in the fifth layer for σ in the OU process. (B)-(F) The examples of time-series to the output value of the OU process.

We visualized the spike coherence of the fifth layer in the inhomogeneous Poisson input in the OU process (page 33) when σ, one of the parameters associated with the input variability, changed (we set parameters of OU process; $\theta = 0.1, \mu = \lambda_{init} = 100$). As a result, the spike coherence of the fifth layer decreased when σ increased. In addition, the time-series change in OU process output averaged over 100 trials were also visualized. We found that the average OU process output of the time series was close to the expected value of the OU process even if the σ changed. It was also shown that when σ is zero, the in-

put of the inhomogeneous mode is equivalent to a homogeneous Poisson process. Therefore, the inhomogeneous mode does not improve spike coherence even when the σ is extremely large, and coherence can be decreased as the σ increases.

References

[1] Annual Reviews. THE EMOTIONS : A History of Changing Outlooks. pp. 1–21, 1993.

[2] Tamara B Franklin, Bechara J Saab, and Isabelle M Mansuy. Neural Mechanisms of Stress Resilience and Vulnerability. *Neuron*, Vol. 75, No. 5, pp. 747–761, 2012.

[3] George P. Chrousos and Philip W. Gold. The Concepts of Stress and Stress System Disorders: Overview of Physical and Behavioral Homeostasis. *JAMA: The Journal of the American Medical Association*, Vol. 267, No. 9, pp. 1244–1252, 1992.

[4] Sabrina Trapp, John P O'Doherty, and Lars Schwabe. Stressful Events as Teaching Signals for the Brain. *Trends in Cognitive Sciences*, Vol. 22, No. 6, pp. 475–478, 2018.

[5] Steven M. Southwick, Meena Vythilingam, and Dennis S. Charney. The psychobiology of depression and resilience to stress: Implications for prevention and treatment. *Annual Review of Clinical Psychology*, Vol. 1, pp. 255–291, 2005.

[6] Christopher Pittenger and Ronald S. Duman. Stress, depression, and neuroplasticity: A convergence of mechanisms. *Neuropsychopharmacology*, Vol. 33, No. 1, pp. 88–109, 2008.

[7] James J Gross and Ross A Thompson. Emotion Regulation: Conceptual Foundations. In *Handbook of emotion regulation.*, pp. 3–24. The Guilford Press, New York, NY, US, 2007.

[8] James J. Gross. Emotion Regulation: Current Status and Future Prospects. *Psychological Inquiry*, Vol. 26, No. 1, pp. 1–26, 2015.

[9] Amit Etkin, Christian Büchel, and James J Gross. The neural bases of emotion regulation. *Nature reviews. Neuroscience*, Vol. 16, No. 11, pp. 693–700, 2015.

[10] Steven M. Pauff and Stephen C. Miller. NIH2 Public Access. *Bone*, Vol. 78, No. 2, pp. 711–716, 2012.

[11] Jason T Buhle, Jennifer A Silvers, Tor D Wager, Richard Lopez, Chukwudi Onyemekwu, Hedy Kober, Jochen Weber, and Kevin N Ochsner. Cognitive Reappraisal of Emotion: A Meta-Analysis of Human Neuroimaging Studies. *Cerebral Cortex*, Vol. 24, No. 11, pp. 2981–2990, 2014.

[12] 2012 Morris et al. 1NIH Public Access. *Gerontology*, Vol. 61, No. 6, pp. 515–525, 2015.

[13] Susan W. White, Donald Oswald, Thomas Ollendick, and Lawrence Scahill. Anxiety in children and adolescents with autism spectrum disorders. *Clinical Psychology Review*, Vol. 29, No. 3, pp. 216–229, 2009.

[14] Amelia Aldao, Susan Nolen-Hoeksema, and Susanne Schweizer. Emotion-regulation strategies across psychopathology: A meta-analytic review. *Clinical Psychology Review*, Vol. 30, No. 2, pp. 217–237, 2010.

[15] Randy L. Buckner, Jessica R. Andrews-Hanna, and Daniel L. Schacter. The brain's default network: Anatomy, function, and relevance to disease. *Annals of the New York Academy of Sciences*, Vol. 1124, pp. 1–38, 2008.

[16] Xiyao Xie, Satja Mulej Bratec, Gabriele Schmid, Chun Meng, Anselm Doll, Afra Wohlschläger, Kathrin Finke, Hans Förstl, Claus Zimmer, Reinhard Pekrun, Leonhard Schilbach, Valentin Riedl, and Christian Sorg. How do you make me feel better? Social cognitive emotion regulation and the default mode network. *NeuroImage*, Vol. 134, pp. 270–280, 2016.

[17] J. van Oort, I. Tendolkar, E. J. Hermans, P. C. Mulders, C. F. Beckmann, A. H. Schene, G. Fernández, and P. F. van Eijndhoven. How the brain

connects in response to acute stress: A review at the human brain systems level. *Neuroscience & Biobehavioral Reviews*, Vol. 83, No. April, pp. 281–297, 2017.

[18] Yawei Cheng, Ching Po Lin, Ho Ling Liu, Yuan Yu Hsu, Kun Eng Lim, Daisy Hung, and Jean Decety. Expertise Modulates the Perception of Pain in Others. *Current Biology*, Vol. 17, No. 19, pp. 1708–1713, 2007.

[19] Meghan L. Meyer, Carrie L. Masten, Yina Ma, Chenbo Wang, Zhenhao Shi, Naomi I. Eisenberger, and Shihui Han. Empathy for the social suffering of friends and strangers recruits distinct patterns of brain activation. *Social Cognitive and Affective Neuroscience*, Vol. 8, No. 4, pp. 446–454, 2013.

[20] Mauricio R. Delgado, Katherine I. Nearing, Joseph E. LeDoux, and Elizabeth A. Phelps. Neural Circuitry Underlying the Regulation of Conditioned Fear and Its Relation to Extinction. *Neuron*, Vol. 59, No. 5, pp. 829–838, 2008.

[21] Anthony S David, Lisette Van Der Meer, and Sergi Costafreda. Neuroscience and Biobehavioral Reviews Self-reflection and the brain : A theoretical review and meta-analysis of neuroimaging studies with implications for schizophrenia. Vol. 34, pp. 935–946, 2010.

[22] Esther Kristina Diekhof, Katharina Geier, Peter Falkai, and Oliver Gruber. Fear is only as deep as the mind allows. A coordinate-based meta-analysis of neuroimaging studies on the regulation of negative affect. *NeuroImage*, Vol. 58, No. 1, pp. 275–285, 2011.

[23] Amy Winecoff, John A. Clithero, R. Mc Kell Carter, Sara R. Bergman, Lihong Wang, and Scott A. Huettel. Ventromedial prefrontal cortex encodes emotional value. *Journal of Neuroscience*, Vol. 33, No. 27, pp. 11032–11039, 2013.

[24] Leah H. Somerville, Dylan D. Wagner, Gagan S. Wig, Joseph M. Moran, Paul J. Whalen, and William M. Kelley. Interactions between transient and sustained neural signals support the generation and regulation of anxious emotion. *Cerebral Cortex*, Vol. 23, No. 1, pp. 49–60, 2013.

[25] Lisette van der Meer, Sergi Costafreda, André Aleman, and Anthony S. David. Self-reflection and the brain: A theoretical review and meta-analysis of neuroimaging studies with implications for schizophrenia. *Neuroscience and Biobehavioral Reviews*, Vol. 34, No. 6, pp. 935–946, 2010.

[26] Chloe E. Page and Laurence Coutellier. Prefrontal excitatory/inhibitory balance in stress and emotional disorders: Evidence for over-inhibition. *Neuroscience and Biobehavioral Reviews*, Vol. 105, No. August, pp. 39–51, 2019.

[27] Stefano Delli Pizzi, Caterina Padulo, Alfredo Brancucci, Giovanna Bubbico, Richard A. Edden, Antonio Ferretti, Raffaella Franciotti, Valerio Manippa, Daniele Marzoli, Marco Onofrj, Gianna Sepede, Armando Tartaro, Luca Tommasi, Stefano Puglisi-Allegra, and Laura Bonanni. GABA content within the ventromedial prefrontal cortex is related to trait anxiety. *Social Cognitive and Affective Neuroscience*, Vol. 11, No. 5, pp. 758–766, 2016.

[28] Stefano Delli Pizzi, Piero Chiacchiaretta, Dante Mantini, Giovanna Bubbico, Antonio Ferretti, Richard A. Edden, Camillo Di Giulio, Marco Onofrj, and Laura Bonanni. Functional and neurochemical interactions within the amygdala-medial prefrontal cortex circuit and their relevance to emotional processing. *Brain Structure and Function*, Vol. 222, No. 3, pp. 1267–1279, 2017.

[29] Stefano Delli Pizzi, Piero Chiacchiaretta, Dante Mantini, Giovanna Bubbico, Richard A. Edden, Marco Onofrj, Antonio Ferretti, and Laura Bonanni. GABA content within medial prefrontal cortex predicts the variability of fronto-limbic effective connectivity. *Brain Structure and Function*, Vol. 222, No. 7, pp. 3217–3229, 2017.

[30] Amanda Kiemes, Cathy Davies, Matthew J. Kempton, Paulina B. Lukow, Carly Bennallick, James M. Stone, and Gemma Modinos. GABA, Glutamate and Neural Activity: A Systematic Review With Meta-Analysis of Multimodal 1H-MRS-fMRI Studies. *Frontiers in Psychiatry*, Vol. 12, No. March, 2021.

[31] Steven F Maier and Linda R Watkins. Role of the medial prefrontal cortex in coping and resilience. *Brain Research*, Vol. 1355, pp. 52–60, 2010.

[32] B. Myers-Schulz and M. Koenigs. Functional anatomy of ventromedial prefrontal cortex: Implications for mood and anxiety disorders. *Molecular Psychiatry*, Vol. 17, No. 2, pp. 132–141, 2012.

[33] Rajita Sinha, Cheryl M Lacadie, R Todd Constable, and Dongju Seo. Dynamic neural activity during stress signals resilient coping. *Proceedings of the National Academy of Sciences*, Vol. 113, No. 31, pp. 8837–8842, 2016.

[34] Daniela Schiller and Mauricio R. Delgado. Overlapping neural systems mediating extinction, reversal and regulation of fear. *Trends in Cognitive Sciences*, Vol. 14, No. 6, pp. 268–276, 2010.

[35] Amit Etkin, Tobias Egner, and Raffael Kalisch. Emotional processing in anterior cingulate and medial prefrontal cortex. *Trends in Cognitive Sciences*, Vol. 15, No. 2, pp. 85–93, 2011.

[36] Jana Campbell and Ulrike Ehlert. Acute psychosocial stress: Does the emotional stress response correspond with physiological responses? *Psychoneuroendocrinology*, Vol. 37, No. 8, pp. 1111–1134, 2012.

[37] Urs M. Nater, Nicolas Rohleder, Wolff Schlotz, Ulrike Ehlert, and Clemens Kirschbaum. Determinants of the diurnal course of salivary alpha-amylase. *Psychoneuroendocrinology*, Vol. 32, No. 4, pp. 392–401, 2007.

[38] Eero Kajantie and David I.W. Phillips. The effects of sex and hormonal status on the physiological response to acute psychosocial stress. *Psychoneuroendocrinology*, Vol. 31, No. 2, pp. 151–178, 2006.

[39] Brigitte M. Kudielka and Clemens Kirschbaum. Sex differences in HPA axis responses to stress: A review. *Biological Psychology*, Vol. 69, No. 1 SPEC. ISS., pp. 113–132, 2005.

[40] C Kirschbaum, K M. Pirke, and D H Hellhammer. The 'Trier Social Stress Test'–A Tool for Investigating Psychobiological Stress Responses in a Laboratory Setting. *Neuropsychobiology*, Vol. 28, No. 1-2, pp. 76–81, 1993.

[41] S Het, N Rohleder, D Schoofs, C Kirschbaum, and O T Wolf. Neuroendocrine and psychometric evaluation of a placebo version of the 'Trier Social Stress Test'. *Psychoneuroendocrinology*, Vol. 34, No. 7, pp. 1075–1086, 2009.

[42] Monika Riegel, Łukasz Żurawski, Małgorzata Wierzba, Abnoss Moslehi, Łukasz Klocek, Marko Horvat, Anna Grabowska, Jarosław Michałowski, Katarzyna Jednoróg, Artur Marchewka, Łukasz Zurawski, Katarzyna Jednoróg, and Anna Grabowska. The Nencki Affective Picture System (NAPS): introduction to a novel, standardized, wide-range, high-quality, realistic picture database. *Behavior research methods*, Vol. 46, No. 2, pp. 600–612, 2014.

[43] Monika Riegel, Łukasz Żurawski, Małgorzata Wierzba, Abnoss Moslehi, Łukasz Klocek, Marko Horvat, Anna Grabowska, Jarosław Michałowski, Katarzyna Jednoróg, and Artur Marchewka. Characterization of the Nencki Affective Picture System by discrete emotional categories (NAPS BE). *Behavior research methods*, Vol. 48, No. 2, pp. 600–612, 2016.

[44] Gorusch T C Spielberger CD and Lushene RE. The State Trait Anxiety Inventory. *Consulting Psychologists Press, Palo Alto, CA.*, 1970.

[45] Hidano T, Fukuhara M, Iwawaki M, Soga S, and Spielberger CD. New STAI Manual State-Trait Anxiety Inventory-Form JYZ. *Jitsumu Kyouiku Press, Tokyo.*, 2000.

[46] Candace M. Raio, Temidayo A. Orederu, Laura Palazzolo, Ashley A. Shurick, and Elizabeth A. Phelps. Cognitive emotion regulation fails the stress test. *Proceedings of the National Academy of Sciences of the United States of America*, Vol. 110, No. 37, pp. 15139–15144, 2013.

[47] Simón Guendelman, Mareike Bayer, Kristin Prehn, and Isabel Dziobek. Regulating negative emotions of others reduces own stress: Neurobiological correlates and the role of individual differences in empathy. *NeuroImage*, Vol. 254, No. April 2021, p. 119134, 2022.

[48] Christian Grillon, Roman Duncko, Matthew F Covington, Lori Kopperman, and Mitchel A Kling. Acute Stress Potentiates Anxiety in Humans. *Biological Psychiatry*, Vol. 62, No. 10, pp. 1183–1186, 2007.

[49] Elaine Fox, Shanna Cahill, and Konstantina Zougkou. Preconscious Processing Biases Predict Emotional Reactivity to Stress. *Biological Psychiatry*, Vol. 67, No. 4, pp. 371–377, 2010.

[50] Meltem Weger and Carmen Sandi. High anxiety trait: A vulnerable phenotype for stress-induced depression. *Neuroscience and Biobehavioral Reviews*, Vol. 87, No. November 2017, pp. 27–37, 2018.

[51] Mohammed R. Milad, Christopher I. Wright, Scott P. Orr, Roger K. Pitman, Gregory J. Quirk, and Scott L. Rauch. Recall of Fear Extinction in Humans Activates the Ventromedial Prefrontal Cortex and Hippocampus in Concert. *Biological Psychiatry*, Vol. 62, No. 5, pp. 446–454, 2007.

[52] Tor D. Wager, Christian E. Waugh, Martin Lindquist, Doug C. Noll, Barbara L. Fredrickson, and Stephan F. Taylor. Brain mediators of cardiovascular responses to social threat. Part I: Reciprocal dorsal and ventral sub-regions of the medial prefrontal cortex and heart-rate reactivity. *NeuroImage*, Vol. 47, No. 3, pp. 821–835, 2009.

[53] Roberto Viviani. Neural Correlates of Emotion Regulation in the Ventral Prefrontal Cortex and the Encoding of Subjective Value and Economic Utility. *Frontiers in Psychiatry*, Vol. 5, No. September, pp. 1–11, 2014.

[54] N Kohn, S B Eickhoff, M Scheller, A R Laird, P T Fox, and U Habel. Neural network of cognitive emotion regulation — An ALE meta-analysis and MACM analysis. *NeuroImage*, Vol. 87, pp. 345–355, 2014.

[55] Tor D. Wager, Matthew L. Davidson, Brent L. Hughes, Martin A. Lindquist, and Kevin N. Ochsner. Prefrontal-Subcortical Pathways Mediating Successful Emotion Regulation. *Neuron*, Vol. 59, No. 6, pp. 1037–1050, 2008.

[56] Antonio R. Damasio, Thomas J. Grabowski, Antoine Bechara, Hanna Damasio, Laura L.B. Ponto, Josef Parvizi, and Richard D. Hichwa. Subcortical and cortical brain activity during the feeling of self-generated emotions. *Nature Neuroscience*, Vol. 3, No. 10, pp. 1049–1056, 2000.

[57] Jens C. Pruessner, Katarina Dedovic, Najmeh Khalili-Mahani, Veronika Engert, Marita Pruessner, Claudia Buss, Robert Renwick, Alain Dagher, Michael J. Meaney, and Sonia Lupien. Deactivation of the Limbic System During Acute Psychosocial Stress: Evidence from Positron Emission Tomography and Functional Magnetic Resonance Imaging Studies. *Biological Psychiatry*, Vol. 63, No. 2, pp. 234–240, 2008.

[58] Kathy Y. Liu, Freya Marijatta, Dorothea Hämmerer, Julio Acosta-Cabronero, Emrah Düzel, and Robert J. Howard. Magnetic resonance imaging of the human locus coeruleus: A systematic review. *Neuroscience and Biobehavioral Reviews*, Vol. 83, No. October, pp. 325–355, 2017.

[59] Gary Aston-Jones, Janusz Rajkowski, and Jonathan Cohen. Role of locus coeruleus in attention and behavioral flexibility. *Biological Psychiatry*, Vol. 46, No. 9, pp. 1309–1320, 1999.

[60] Craig W. Berridge and Barry D. Waterhouse. The locus coeruleus-noradrenergic system: Modulation of behavioral state and state-dependent cognitive processes. *Brain Research Reviews*, Vol. 42, No. 1, pp. 33–84, 2003.

[61] Susan J. Sara. The locus coeruleus and noradrenergic modulation of cognition. *Nature Reviews Neuroscience*, Vol. 10, No. 3, pp. 211–223, 2009.

[62] Adriana Feder, Eric J Nestler, and Dennis S Charney. Psychobiology and molecular genetics of resilience. *Nature reviews. Neuroscience*, Vol. 10, No. 6, pp. 446–457, 2009.

[63] Nikos Priovoulos, Heidi I L Jacobs, Dimo Ivanov, Kâmil Uludaˇg, Frans R J Verhey, and Benedikt A Poser. High-resolution in vivo imaging of human locus coeruleus by magnetization transfer MRI at 3T and 7T. *NeuroImage*, Vol. 168, pp. 427–436, 2018.

[64] Laura J. Julian. Measures of anxiety: State-Trait Anxiety Inventory (STAI), Beck Anxiety Inventory (BAI), and Hospital Anxiety and Depression Scale-Anxiety (HADS-A). *Arthritis Care and Research*, Vol. 63, No. SUPPL. 11, pp. 467–472, 2011.

[65] Amy F T Arnsten. Stress signalling pathways that impair prefrontal cortex structure and function. *Nature Reviews Neuroscience*, Vol. 10, No. 6, pp. 410–422, 2009.

[66] Heather L. Urry, Carien M. Van Reekum, Tom Johnstone, Ned H. Kalin, Marchell E. Thurow, Hillary S. Schaefer, Cory A. Jackson, Corrina J. Frye, Lawrence L. Greischar, Andrew L. Alexander, and Richard J. Davidson. Amygdala and ventromedial prefrontal cortex are inversely coupled during regulation of negative affect and predict the diurnal pattern of cortisol secretion among older adults. *Journal of Neuroscience*, Vol. 26, No. 16, pp. 4415–4425, 2006.

[67] Melissa R. Warden, Aslihan Selimbeyoglu, Julie J. Mirzabekov, Maisie Lo, Kimberly R. Thompson, Sung Yon Kim, Avishek Adhikari, Kay M. Tye, Loren M. Frank, and Karl Deisseroth. A prefrontal cortex-brainstem neuronal projection that controls response to behavioural challenge. *Nature*, Vol. 492, No. 7429, pp. 428–432, 2012.

[68] Akira Uematsu, Bao Zhen Tan, Edgar A Ycu, Jessica Sulkes Cuevas, Jenny Koivumaa, Felix Junyent, Eric J Kremer, Ilana B Witten, Karl Deisseroth, and Joshua P Johansen. Modular organization of the brainstem noradrenaline system coordinates opposing learning states. *Nature Neuroscience*, Vol. 20, No. 11, pp. 1602–1611, 2017.

[69] Paul J. Whalen, Hannah Raila, Randi Bennett, Alison Mattek, Annemarie Brown, James Taylor, Michelle Van Tieghem, Alexandra Tanner, Matthew Miner, and Amy Palmer. Neuroscience and facial expressions of emotion: The role of amygdala-prefrontal interactions. *Emotion Review*, Vol. 5, No. 1, pp. 78–83, 2013.

[70] James J. Gross and Ricardo F. Muñoz. Emotion Regulation and Mental Health. *Clinical Psychology: Science and Practice*, Vol. 2, No. 2, pp. 151–164, 1995.

[71] James J. Gross and Hooria Jazaieri. Emotion, emotion regulation, and psychopathology: an affective science perspective. *Clinical Psychological Science*, Vol. 2, No. 4, pp. 387–401, 2014.

[72] Sonia Torres-Sanchez, Laura Perez-Caballero, Juan A Mico, Pau Celada, and Esther Berrocoso. Effect of Deep Brain Stimulation of the ventromedial prefrontal cortex on the noradrenergic system in rats. *Brain Stimulation: Basic, Translational, and Clinical Research in Neuromodulation*, Vol. 11, No. 1, pp. 222–230, 2018.

[73] Fukuda Megumi, Ayumu Yamashita, Mitsuo Kawato, and Hiroshi Imamizu. Functional MRI neurofeedback training on connectivity between two regions induces long-lasting changes in intrinsic functional network. *Frontiers in Human Neuroscience*, Vol. 9, No. MAR, 2015.

[74] Takashi Yamada, Ryu Ichiro Hashimoto, Noriaki Yahata, Naho Ichikawa, Yujiro Yoshihara, Yasumasa Okamoto, Nobumasa Kato, Hidehiko Takahashi, and Mitsuo Kawato. Resting-state functional connectivity-based biomarkers and functional mri-based neurofeedback for psychiatric disorders: A challenge for developing theranostic biomarkers. *International Journal of Neuropsychopharmacology*, Vol. 20, No. 10, pp. 769–781, 2017.

[75] George A. Bonanno and Charles L. Burton. Regulatory Flexibility: An Individual Differences Perspective on Coping and Emotion Regulation. *Perspectives on Psychological Science*, Vol. 8, No. 6, pp. 591–612, 2013.

[76] Peter Smittenaar, Thomas H.B. FitzGerald, Vincenzo Romei, Nicholas D. Wright, and Raymond J. Dolan. Disruption of Dorsolateral Prefrontal Cortex Decreases Model-Based in Favor of Model-free Control in Humans. *Neuron*, Vol. 80, No. 4, pp. 914–919, 2013.

[77] A Ross Otto, Candace M Raio, Alice Chiang, Elizabeth A Phelps, and Nathaniel D Daw. Working-memory capacity protects model-based learning

from stress. *Proceedings of the National Academy of Sciences*, Vol. 110, No. 52, pp. 20941–20946, 2013.

[78] Daniela Schoofs, Oliver T Wolf, and Tom Smeets. Cold pressor stress impairs performance on working memory tasks requiring executive functions in healthy young men. *Behavioral neuroscience*, Vol. 123, No. 5, pp. 1066–1075, 2009.

[79] Shaozheng Qin, Erno J Hermans, Hein J F van Marle, Jing Luo, and Guillén Fernández. Acute Psychological Stress Reduces Working Memory-Related Activity in the Dorsolateral Prefrontal Cortex. *Biological Psychiatry*, Vol. 66, No. 1, pp. 25–32, 2009.

[80] Herbert Bless, Tilmann Betsch, and Axel Franzen. Framing the framing effect: The impact of context cues on solutions to the 'Asian disease' problem. *European Journal of Social Psychology*, Vol. 28, No. 2, pp. 287–291, 1998.

[81] Erno J Hermans, Marloes J A G Henckens, Marian Joëls, and Guillén Fernández. Dynamic adaptation of large-scale brain networks in response to acute stressors. *Trends in Neurosciences*, Vol. 37, No. 6, pp. 304–314, 2014.

[82] N. F. Narvaez Linares, V. Charron, A. J. Ouimet, P. R. Labelle, and H. Plamondon. A systematic review of the Trier Social Stress Test methodology: Issues in promoting study comparison and replicable research. *Neurobiology of Stress*, Vol. 13, p. 100235, 2020.

[83] Bruce S. McEwen and John H. Morrison. The brain on stress: vulnerability and plasticity of the prefrontal cortex over the life course. *Neuron*, Vol. 79, No. 1, pp. 16–29, 2013.

[84] Gregor Domes, Lars Schulze, Moritz Böttger, Annette Grossmann, Karlheinz Hauenstein, Petra H. Wirtz, Markus Heinrichs, and Sabine C. Herpertz. The neural correlates of sex differences in emotional reactivity and emotion regulation. *Human Brain Mapping*, Vol. 31, No. 5, pp. 758–769, 2010.

[85] Seung Hee Lee and Yang Dan. Neuromodulation of Brain States. *Neuron*, Vol. 76, No. 1, pp. 209–222, 2012.

[86] Susan J. Sara and Sebastien Bouret. Orienting and Reorienting: The Locus Coeruleus Mediates Cognition through Arousal. *Neuron*, Vol. 76, No. 1, pp. 130–141, 2012.

[87] Gary Aston-Jones, Matthew Ennis, Vincent A. Pieribone, W. Thompson Nickell, and Michael T. Shipley. The brain nucleus locus coeruleus: Restricted afferent control of a broad efferent network. *Science*, Vol. 234, No. 4777, pp. 734–737, 1986.

[88] S L Foote and J H Morrison. Extrathalamic Modulation of Cortical Function. *Annual Review of Neuroscience*, Vol. 10, No. 1, pp. 67–95, 1987.

[89] Andrea Bari, Sangyu Xu, Michele Pignatelli, Daigo Takeuchi, Jiesi Feng, Yulong Li, and Susumu Tonegawa. Differential attentional control mechanisms by two distinct noradrenergic coeruleo-frontal cortical pathways. *Proceedings of the National Academy of Sciences of the United States of America*, Vol. 117, No. 46, pp. 29080–29089, 2020.

[90] Nicole A. Aponte-Santiago and J. Troy Littleton. Synaptic Properties and Plasticity Mechanisms of Invertebrate Tonic and Phasic Neurons. *Frontiers in Physiology*, Vol. 11, No. December, pp. 1–19, 2020.

[91] David M. Devilbiss and Barry D. Waterhouse. Phasic and tonic patterns of locus coeruleus output differentially modulate sensory network function in the awake rat. *Journal of Neurophysiology*, Vol. 105, No. 1, pp. 69–87, 2011.

[92] Abhinaba Ghosh, Faghihe Massaeli, Kyron D Power, Tamunotonye Omoluabi, Sarah E Torraville, Julia B Pritchett, Tayebeh Sepahvand, Vanessa D Strong, Camila Reinhardt, Xihua Chen, Gerard M Martin, Carolyn W Harley, and Qi Yuan. Locus Coeruleus Activation Patterns Differentially Modulate Odor Discrimination Learning and Odor Valence in Rats. *Cerebral Cortex Communications*, Vol. 2, No. 2, pp. 1–17, 2021.

[93] Elena M. Vazey, David E. Moorman, and Gary Aston-Jones. Phasic locus coeruleus activity regulates cortical encoding of salience information. *Proceedings of the National Academy of Sciences of the United States of America*, Vol. 115, No. 40, pp. E9439–E9448, 2018.

[94] Matthew E. Carter, Ofer Yizhar, Sachiko Chikahisa, Hieu Nguyen, Antoine Adamantidis, Seiji Nishino, Karl Deisseroth, and Luis De Lecea. Tuning arousal with optogenetic modulation of locus coeruleus neurons. *Nature Neuroscience*, Vol. 13, No. 12, pp. 1526–1535, 2010.

[95] Tamunotonye Omoluabi, Kyron D Power, Tayebeh Sepahvand, Qi Yuan, and Barbara Jane Morley. Phasic and Tonic Locus Coeruleus Stimulation Associated Valence Learning Engages Distinct Adrenoceptors in the Rat Basolateral Amygdala. Vol. 16, No. May, pp. 1–9, 2022.

[96] Gary Aston-Jones and Jonathan D. Cohen. An integrative theory of locus coeruleus-norepinephrine function: Adaptive gain and optimal performance. *Annual Review of Neuroscience*, Vol. 28, pp. 403–450, 2005.

[97] Rita J. Valentino and Elisabeth Van Bockstaele. Convergent regulation of locus coeruleus activity as an adaptive response to stress. *European Journal of Pharmacology*, Vol. 583, No. 2-3, pp. 194–203, 2008.

[98] Erno J. Hermans, Marloes J.A.G. Henckens, Marian Joëls, and Guillén Fernández. Dynamic adaptation of large-scale brain networks in response to acute stressors. *Trends in Neurosciences*, Vol. 37, No. 6, pp. 304–314, 2014.

[99] Sarah C. Kelly, Bin He, Sylvia E. Perez, Stephen D. Ginsberg, Elliott J. Mufson, and Scott E. Counts. Locus coeruleus cellular and molecular pathology during the progression of Alzheimer's disease. *Acta neuropathologica communications*, Vol. 5, No. 1, p. 8, 2017.

[100] Niels Hansen. Locus Coeruleus Malfunction Is Linked to Psychopathology in Prodromal Dementia With Lewy Bodies. *Frontiers in Aging Neuroscience*, Vol. 13, No. March, pp. 1–8, 2021.

[101] Shristi Baral, Hassan Hosseini, Kaushik More, Thomaz M. C. Fabrin, Jochen Braun, and Matthias Prigge. Spike-Dependent Dynamic Partitioning of the Locus Coeruleus Network through Noradrenergic Volume Release in a Simulation of the Nucleus Core. *Brain Sciences*, Vol. 12, No. 6, p. 728, 2022.

[102] Anna C. Sales, Karl J. Friston, Matthew W. Jones, Anthony E. Pickering, and Rosalyn J. Moran. Locus Coeruleus tracking of prediction errors optimises cognitive flexibility: An Active Inference model. *bioRxiv*, pp. 1–24, 2018.

[103] Eric Shea-Brown, Mark S. Gilzenrat, and Jonathan D. Cohen. Optimization of decision making in multilayer networks: The role of locus coeruleus. *Neural Computation*, Vol. 20, No. 12, pp. 2863–2894, 2008.

[104] D Mumford. On the computational architecture of the neocortex. I. The role of the thalamo-cortical loop. *Biological cybernetics*, Vol. 65, No. 2, pp. 135–145, 1991.

[105] Dean V. Buonomano and Wolfgang Maass. State-dependent computations: Spatiotemporal processing in cortical networks. *Nature Reviews Neuroscience*, Vol. 10, No. 2, pp. 113–125, 2009.

[106] Rodney J. Douglas and Kevan A.C. Martin. Neuronal circuits of the neocortex. *Annual Review of Neuroscience*, Vol. 27, No. 13, pp. 419–451, 2004.

[107] Rodney J. Douglas and Kevan A.C. Martin. Mapping the matrix: the ways of neocortex. *Neuron*, Vol. 56, No. 2, pp. 226–238, 2007.

[108] Kenneth D. Harris and Alexander Thiele. Cortical state and attention. *Nature Reviews Neuroscience*, Vol. 12, No. 9, pp. 509–523, 2011.

[109] Petr Maršálek, Christof Koch, and John Maunsell. On the relationship between synaptic input and spike output jitter in individual neurons. *Proceedings of the National Academy of Sciences of the United States of America*, Vol. 94, No. 2, pp. 735–740, 1997.

[110] Shuzo Sakata and Kenneth D. Harris. Laminar Structure of Spontaneous and Sensory-Evoked Population Activity in Auditory Cortex. *Neuron*, Vol. 64, No. 3, pp. 404–418, 2009.

[111] Tatjana Tchumatchenko, Aleksey Malyshev, Fred Wolf, and Maxim Volgushev. Ultrafast population encoding by cortical neurons. *Journal of Neuroscience*, Vol. 31, No. 34, pp. 12171–12179, 2011.

[112] Yuichi Sakumura and Shin Ishii. Stochastic resonance with differential code in feedforward network with intra-layer random connections. *Neural Networks*, Vol. 19, No. 4, pp. 469–476, 2006.

[113] David Heeger. Poisson Model of Spike Generation. *Handout*, pp. 1–13, 2000.

[114] Luigi M. Ricciardi and Laura Sacerdote. The Ornstein-Uhlenbeck process as a model for neuronal activity. *Biological Cybernetics*, Vol. 35, No. 1, pp. 1–9, 1979.

[115] A L HODGKIN and A F HUXLEY. A quantitative description of membrane current and its application to conduction and excitation in nerve. *The Journal of physiology*, Vol. 117, No. 4, pp. 500–544, aug 1952.

[116] R. Fitzhugh. Theoretical effect of temperature on threshold in the Hodgkin-Huxley nerve model. *The Journal of general physiology*, Vol. 49, No. 5, pp. 989–1005, 1966.

[117] T. H. Brown and D. Johnston. Voltage-clamp analysis of mossy fiber synaptic input to hippocampal neurons. *Journal of Neurophysiology*, Vol. 50, No. 2, pp. 487–507, 1983.

[118] Anthony Zador, Christof Koch, and Thomas H. Brown. Biophysical model of a Hebbian synapse. *Proceedings of the National Academy of Sciences of the United States of America*, Vol. 87, No. 17, pp. 6718–6722, 1990.

[119] H. Câteau and T. Fukai. Fokker-Planck approach to the pulse packet propagation in synfire chain. *Neural Networks*, Vol. 14, No. 6-7, pp. 675–685, 2001.

[120] Marius Usher, Jonathan D. Cohen, David Servan-Schreiber, Janusz Rajkowski, and Gary Aston-Jones. The role of locus coeruleus in the regulation of cognitive performance. *Science*, Vol. 283, No. 5401, pp. 549–554, 1999.

[121] Iñigo Arandia-Romero, Seiji Tanabe, Jan Drugowitsch, Adam Kohn, and Rubén Moreno-Bote. Multiplicative and Additive Modulation of Neuronal Tuning with Population Activity Affects Encoded Information. *Neuron*, Vol. 89, No. 6, pp. 1305–1316, 2016.

[122] Mingyu Yang, Nikos K. Logothetis, and Oxana Eschenko. Phasic activation of the locus coeruleus attenuates the acoustic startle response by increasing cortical arousal. *Scientific Reports*, Vol. 11, No. 1, pp. 1–14, 2021.

[123] Kathrin Janitzky. Impaired Phasic Discharge of Locus Coeruleus Neurons Based on Persistent High Tonic Discharge—A New Hypothesis With Potential Implications for Neurodegenerative Diseases. *Frontiers in Neurology*, Vol. 11, No. May, pp. 1–15, 2020.

[124] Peter Dayan and Angela J. Yu. Phasic norepinephrine: A neural interrupt signal for unexpected events. *Network: Computation in Neural Systems*, Vol. 17, No. 4, pp. 335–350, 2006.

[125] David M. Devilbiss. Consequences of tuning network function by tonic and phasic locus coeruleus output and stress: Regulating detection and discrimination of peripheral stimuli. *Brain Research*, Vol. 1709, pp. 16–27, 2019.

[126] Vincent Breton-Provencher, Gabrielle T. Drummond, and Mriganka Sur. Locus Coeruleus Norepinephrine in Learned Behavior: Anatomical Modularity and Spatiotemporal Integration in Targets. *Frontiers in Neural Circuits*, Vol. 15, No. June, pp. 1–11, 2021.

[127] Ana Raquel O. Martins and Robert C. Froemke. Coordinated forms of noradrenergic plasticity in the locus coeruleus and primary auditory cortex. *Nature Neuroscience*, Vol. 18, No. 10, pp. 1483–1492, 2015.

[128] Tamunotonye Omoluabi, Sarah E. Torraville, Aida Maziar, Abhinaba Ghosh, Kyron D. Power, Camila Reinhardt, Carolyn W. Harley, and Qi Yuan. Novelty- like activation of locus coeruleus protects against deleterious human pretangle tau effects while stress- inducing activation worsens its effects. *Alzheimer's & Dementia: Translational Research & Clinical Interventions*, Vol. 7, No. 1, pp. 1–13, 2021.

[129] Jaymar Soriano, Takatomi Kubo, Takao Inoue, Hiroyuki Kida, Toshitaka Yamakawa, Michiyasu Suzuki, and Kazushi Ikeda. Differential temperature sensitivity of synaptic and firing processes in a neural mass model of epileptic discharges explains heterogeneous response of experimental epilepsy to focal brain cooling. *PLoS Computational Biology*, Vol. 13, No. 10, pp. 1–26, 2017.

[130] Gregory J. Quirk, Gregory K. Russo, Jill L. Barron, and Kelimer Lebron. The role of ventromedial prefrontal cortex in the recovery of extinguished fear. *Journal of Neuroscience*, Vol. 20, No. 16, pp. 6225–6231, 2000.

[131] Mauricio R. Delgado, Jennifer S. Beer, Lesley K. Fellows, Scott A. Huettel, Michael L. Platt, Gregory J. Quirk, and Daniela Schiller. Viewpoints: Dialogues on the functional role of the ventromedial prefrontal cortex. *Nature Neuroscience*, Vol. 19, No. 12, pp. 1545–1552, 2016.

[132] Thomas Liebe, Jörn Kaufmann, Meng Li, Martin Skalej, Gerd Wagner, and Martin Walter. In vivo anatomical mapping of human locus coeruleus functional connectivity at 3 T MRI. *Human Brain Mapping*, Vol. 41, No. 8, pp. 2136–2151, 2020.

[133] Tanemichi Chiba, Tetsuro Kayahara, and Katsuma Nakano. Efferent projections of infralimbic and prelimbic areas of the medial prefrontal cortex in the Japanese monkey, Macaca fuscata. *Brain Research*, Vol. 888, No. 1, pp. 83–101, 2001.

[134] Yuefeng Lu, Kimberly L. Simpson, Kristin J. Weaver, and Rick C.S. Lin. Differential Distribution Patterns From Medial Prefrontal Cortex and Dorsal Raphe to the Locus Coeruleus in Rats. *Anatomical Record*, Vol. 295, No. 7, pp. 1192–1201, 2012.

[135] Susan J. Sara and Anne Hervé-Minvielle. Inhibitory influence of frontal cortex on locus coeruleus neurons. *Proceedings of the National Academy of Sciences of the United States of America*, Vol. 92, No. 13, pp. 6032–6036, 1995.

[136] Sheng Zhang, Sien Hu, Herta H. Chao, and Chiang Shan R. Li. Resting-State Functional Connectivity of the Locus Coeruleus in Humans: In Comparison with the Ventral Tegmental Area/Substantia Nigra Pars Compacta and the Effects of Age. *Cerebral Cortex*, Vol. 26, No. 8, pp. 3413–3427, 2016.